Theor Chem Acc (2014) 133:1405
DOI 10.1007/s00214-013-1405-1

FEATURE ARTICLE

How to choose the frozen density in Frozen-Density Embedding Theory-based numerical simulations of local excitations?

Marie Humbert-Droz · Xiuwen Zhou · Sapana V. Shedge · Tomasz A. Wesolowski

Received: 2 July 2013 / Accepted: 2 October 2013 / Published online: 6 November 2013

Abstract According to Frozen-Density Embedding Theory, any observable evaluated for the embedded species is a functional of the frozen density (ρ_B—the density associated with the environment). The environment-induced shifts in the energies of local excitations in organic chromophores embedded in hydrogen-bonded environments are analyzed. The excitation energies obtained for ρ_B, which is derived from ground-state calculations for the whole environment applying medium quality basis sets (STO–DZP) or larger, vary in a narrow range (about 0.02 eV which is at least one order of magnitude less than the magnitude of the shift). At the same time, the ground-state dipole moment of the environment varies significantly. The lack of correlation between the calculated shift and the dipole moment of the environment reflects the fact that, in Frozen-Density Embedding Theory, the partitioning of the total density is not unique. As a consequence, such concepts as "environment polarization" are not well defined within Frozen-Density Embedding Theory. Other strategies to generate ρ_B (superposition of densities of atoms/molecules in the environment) are shown to be less robust for simulating excitation energy shifts for chromophores in environments comprising hydrogen-bonded molecules.

Keywords Frozen-Density Embedding Theory · Linear-response time-dependent density functional theory · Solvatochromism · Molecular clusters · Multi-level simulations

Electronic supplementary material The online version of this article (doi:10.1007/s00214-013-1405-1) contains supplementary material, which is available to authorized users.

M. Humbert-Droz · X. Zhou · S. V. Shedge · T. A. Wesolowski (✉)
Département de Chimie Physique, Université de Genève, 30, quai Ernest-Ansermet, 1211 Geneva 4, Switzerland
e-mail: Tomasz.Wesolowski@unige.ch

1 Introduction

The use of local potentials to couple a system described at quantum mechanical level with its environment has a long history in quantum chemistry. A large majority of methods use electrostatic potentials to this end (for review see Refs. [1–5]). The energy components not represented in the embedding potential are added as a posteriori corrections known under the name as exchange-repulsion. The use of electrostatic-only embedding potential leads, however, to well known problems such as spurious leak of charge density from the embedded subsystem to environment [6, 7] or erratic behavior of the results if the basis set changes [8, 9]. This problem originates from the fact that limiting the embedding potential to its electrostatic component neglects the Pauli exclusion principle (Pauli repulsion or confinement effects). These formal deficiencies of electrostatic-only embedding potentials, which show up in fully variational calculations (see for instance Refs. [8, 9]), are usually dealt with in a pragmatic manner. Atomic basis sets are centered only on the atoms of the embedded systems not the environment (Refs. [1–5]). As a result, the quality of the embedding potential near the nuclei of the environment plays a secondary role. Moreover, the net atomic charges (or sometimes multipoles) are used to generate the electrostatic potential. The use of net charges instead of exact total electric charge (negative) and the total nuclear charge (singular and positive) results in less attractive electrostatic potential near the nuclei in the environment. As a result, the possible unphysical distribution of the electron density between the embedded system and its

environment is less likely to take place. In the structurally flexible environment, the non-physical solutions due to the neglect of the Pauli repulsion in the embedding potential can be avoided by using the statistically averaged electrostatic potential [10–12]. Averaging of the fluctuating position of positively charged centers in the environment results in the electrostatic potential being smeared out over extended larger space. The averaged electrostatic potential is less attractive and leads to better numerical stability of the results with respect to the basis set used in variational calculations. An alternative solution to the problem of numerical instabilities originating from the neglect of Pauli repulsion consists of attenuating the Coulomb terms near the nuclei of the atoms in the environment [7] or imposing that the electron density near nuclei in the environment disappears [6]. The resulting additional terms in the embedding potential in such methods can be seen as simple local pseudopotentials (see below). Last but not least, most applications of methods applying electrostatic-only embedding potential aim at obtaining the key parameters of the ground-state potential energy surface of relevance to reactivity and/or conformational equilibria. In such a case, the energy of the system is corrected by terms added a posteriori [1–5], which are usually associated with exchange-repulsion, dispersion, and/or charge transfer represented by empirically parametrized energy contributions or terms derived from first principles [13–15]. As a result, the energy of the embedded system and its wavefunction (or a similar quantum mechanical descriptor such as a wavefunction of the reference non-interacting system used in DFT-based methods) are not self-consistent.

At the formal level, there are two ways to go beyond electrostatic-only embedding potentials in order to take into account the fermion statistics of electrons and obtain both the energy and the wavefunction which are self-consistent. Either by the use of projection operators (constructed as pseudopotentials or frozen orbitals) enforcing Pauli exclusion principle for all electrons in the whole system [5, 6, 16–19] or by the use of the non-electrostatic components in the coupling potential terms derived in Frozen-Density Embedding Theory[1] (FDET) [20–23]. The first strategy involves non-local operators and requires that the quantum mechanical descriptors, i.e., pseudopotentials or frozen orbitals, are used also for the environment. The FDET strategy, on the other hand, involves approximating some terms in the embedding potentials by means of bi-functionals depending on the charge densities associated with the embedded subsystem and the environment. Additional key issue in FDET-based simulations, which is dealt with in detail in the present work, is the choice of the frozen electron density associated with the environment (throughout this work, $\rho_B(\mathbf{r})$ denotes this component of the total electron density). Each of these two strategies has its optimal domains of applicability. The pseudopotential strategy is commonly applied to represent an environment which is a solid. For each element and oxidation state, a transferable pseudopotential can be constructed [18, 19]. For environment, which consists of molecules, the pseudopotential or frozen orbital strategies require constructing transferable pseudopotentials for each molecule (or molecular fragment) [5, 16, 17]. Concerning the FDET strategy, however, the domain of possible applications is determined by the availability of acceptable approximation for the bi-functionals by means of which the embedding potential is expressed and by the availability of an adequate inexpensive procedure to generate an adequate electron density of the environment (ρ_B).

In view of the increasing interest in using FDET-based numerical simulation methods [24–29, 31–33], this work focuses on the dependence of FDET results on $\rho_B(\mathbf{r})$ (for a recent comprehensive review see [30]). Some information about the dependency of the properties of embedded system on ρ_B can be found in the literature [34–43]. A comprehensive and systematic investigation of such dependencies was, however, not reported so far. Here we focus on the evaluation of environment-induced shifts in the energies of local excitations evaluated following the method based on generalization of the linear-response time-dependent DFT strategy [44] for responding systems embedded in a frozen density [37]. Within Neglect of Dynamic Response of the Environment (NDRE) approximation, the quality of such shifts is entirely determined by the accuracy of the embedding potential. If NDRE approximation cannot be applied, as in the case of environment and embedded subsystem absorbing at similar frequency, the method based on generalization of ground-state subsystem DFT [45] is indispensable as shown comprehensively in Ref. [46]. The systems considered in the present work concern environments and chromophores, which do not absorb in the same spectral range, i.e., cases where NDRE approximation can be applied. Note that FDET calculations in which NDRE approximation is applied are also referred to as uncoupled FDE or FDE(u) in the literature [46]. The other approximation made in any FDET-based calculations concerns the non-additive kinetic potential (see the next section). The present work does not concern this approximation. We build up upon the gathered numerical experience reported in the literature. The investigated systems are the same or very similar to the ones for which the adequacy of the used approximations was already put to scrutiny.

[1] In the present work any reference to Density Functional Theory (DFT), subsystem DFT, Kohn–Sham DFT, and Frozen-Density Embedding Theory (FDET), concerns the exact formalisms and not approximate methods based on such formalisms.

The present work is organized as follows. We start with a nutshell presentation of Frozen-Density Embedding Theory which is followed by the overview of the literature concerning the dependence of the FDET results on the choice of the frozen density. A dedicated section deals with the issue of electronic polarization of the environment seen from the FDET perspective. The results section deals with the dependence on energies of local excitations on the chosen ρ_B. In the first part, clusters consisting of *cis*-7-hydroxyquinoline (7HQ) and from one-to three hydrogen-bonded molecules are used to test three strategies to generate ρ_B (superposition of atomic densities, superposition of molecular densities, ground-state Kohn–Sham calculations for the whole environment). For these clusters, shifts of the excitation energies obtained in gas-phase experiments, benchmark quality EOM–FDET (for the smallest ones only) and FDET/LR-TDDFT calculations are available (see data collected in Refs. [8, 47]). These three types of shifts do not differ from each other significantly and provide reference data to investigate the effect of the choice of ρ_B in the FDET/LR-TDDFT calculations. The second part of the results section concerns larger systems, for which the third strategy to generate the frozen density is applied extensively and the effect of varying ρ_B on the calculated shifts is investigated in detail.

1.1 Frozen-Density Embedding Theory

Frozen-Density Embedding Theory [20–23] concerns minimizing the total energy for a system comprising N_{AB} electrons in the external potential $v(\mathbf{r})$ in the presence of the constraint $\rho \geq \rho_B$:

$$E_{\mathrm{emb}}[\rho_B] = \min_{\substack{\rho(\mathbf{r}) \geq \rho_B(\mathbf{r}) \geq 0 \\ \int \rho(\mathbf{r})\mathrm{d}\mathbf{r} = N_{AB}}} E_v^{\mathrm{HK}}[\rho] \tag{1}$$

where $E_v^{\mathrm{HK}}[\rho]$ is the Hohenberg–Kohn functional of the total energy [48] and ρ_B is a given function.

There are no other constraints for $\rho_B(\mathbf{r})$ than the ones given in Eq. 1. If the integral $\int \rho_B(\mathbf{r})\mathrm{d}\mathbf{r}$ is an integer (denoted by N_B) then the difference $N_A = N_{AB} - N_B$ is also an integer, and the above definition can be written alternatively:

$$E_{\mathrm{emb}}[\rho_B] = \min_{\substack{\rho_A(\mathbf{r}) \geq 0 \\ \int \rho_A(\mathbf{r})\mathrm{d}\mathbf{r} = N_A}} E_v^{\mathrm{HK}}[\rho_A + \rho_B] \tag{2}$$

We mention here the closely related formal framework of partition DFT [49, 50], in which the integrals $\int \rho_A(\mathbf{r})\mathrm{d}\mathbf{r}$ and $\int \rho_B(\mathbf{r})\mathrm{d}\mathbf{r}$ can be fractional numbers which add up to an integer (N_{AB}). In FDET, the integral $\int \rho_B(\mathbf{r})\mathrm{d}\mathbf{r}$ can be also a fractional number. In such a case, however, the definition of $E_{\mathrm{emb}}[\rho_B]$ given in Eq. 2 is not applicable and $E_{\mathrm{emb}}[\rho_B]$ is only defined in Eq. 1. FDET provides a practical strategy to perform such a search by constructing an appropriate embedding potential ($v_{\mathrm{emb}}(\mathbf{r})$) assuring satisfaction of the constraint $\rho \geq \rho_B$. The embedding potential is determined uniquely by the following quantities: electron density of the environment (denoted as ρ_B throughout this work), electron density of the embedded system ($\rho_A(\mathbf{r}) = \rho(\mathbf{r}) - \rho_B(\mathbf{r}) \geq 0$ by construction), and the density of the positive charge of the environment ($\rho_B^{\mathrm{pos}}(\mathbf{r})$ is usually the sum of nuclear charges) which generates the electrostatics potential $v_B(\mathbf{r}) = \int \frac{\rho_B^{\mathrm{pos}}(\mathbf{r}')}{|\mathbf{r}'-\mathbf{r}|}\mathrm{d}\mathbf{r}'$. The form of this correspondence was derived for embedding various quantum mechanical systems: reference system of non-interacting electrons (the Kohn–Sham system [51]) [20, 21], interacting wavefunction [22], and one-particle reduced density matrix [23] and reads:[2]

$$v_{\mathrm{emb}}[\rho_A, \rho_B, v_B](\mathbf{r}) = v_B(\mathbf{r}) + \int \frac{\rho_B(\mathbf{r}')}{|\mathbf{r}' - \mathbf{r}|}\mathrm{d}\mathbf{r}' + \frac{\delta E_{\mathrm{xc}}^{\mathrm{nad}}[\rho_A, \rho_B]}{\delta \rho_A(\mathbf{r})} + \frac{\delta T_s^{\mathrm{nad}}[\rho_A, \rho_B]}{\delta \rho_A(\mathbf{r})} \tag{3}$$

The non-additive bi-functionals occurring in the last two terms in the above equation are defined through the functionals for the exchange-correlation energy $E_{\mathrm{xc}}[\rho]$ and for the kinetic energy in the non-interacting reference system $T_s[\rho]$ known in Kohn–Sham formulation of Density Functional Theory [48, 51]. In particular, the constrained search definition [53, 54] of the bi-functional $T_s^{\mathrm{nad}}[\rho_A, \rho_B]$ reads:

$$T_s^{\mathrm{nad}}[\rho_A, \rho_B] = \min_{\Psi_s \to \rho_A + \rho_B} \langle \Psi_s | \hat{T} | \Psi_s \rangle - \min_{\Psi_s \to \rho_A} \langle \Psi_s | \hat{T} | \Psi_s \rangle - \min_{\Psi_s \to \rho_B} \langle \Psi_s | \hat{T} | \Psi_s \rangle \tag{4}$$

where, Ψ_s denotes a trial function of the form of a single-determinant. The index s used in $T_s[\rho]$ and all subsequently defined quantities is used to indicate that the concerned definitions involve the reference system of non-interacting electrons for which the ground-state wavefunction has this form.

In practice, the quality of calculated environment-induced shifts of a given property of the embedded system obtained from FDET-based multi-level simulations, which is calculated either as the expectation value of the operator associated to this property or from response theory-based calculations using embedded wavefunction (like FDET/

[2] In the case of embedded interacting wavefunction of the truncated Configuration Interaction form, an additional term in the embedding potential is needed [22] but it is a matter of convention whether this term is considered a part of the embedding potential or the potential for subsystem A (see also the relevant discussion in Ref. [52]).

LR-TDDFT calculations reported in the present work) hinges on the following factors: (1) choice of $\rho_B(\mathbf{r})$ (electron density of the environment), (2) approximation for the bifunctional $\frac{\delta E_{\mathrm{xc}}^{\mathrm{nad}}[\rho_A,\rho_B]}{\delta\rho_A(\mathbf{r})}$ (the exchange-correlation part in the RHS of Eq. 3 denoted by $v_{\mathrm{xc}}^{\mathrm{nad}}[\rho_A,\rho_B](\mathbf{r})$ in the present work), (3) approximation for the bifunctional $\frac{\delta T_s^{\mathrm{nad}}[\rho_A,\rho_B]}{\delta\rho_A(\mathbf{r})}$ denoted by $v_t^{\mathrm{nad}}[\rho_A,\rho_B](\mathbf{r})$ in the present work. It is worthwhile noticing that the quality of the energy, on the other hand, depends additionally on the error in the functionals used to generate the embedding potential (for the detailed discussion see Ref. [55]).

This work focuses on the first issue. Concerning approximating $v_t^{\mathrm{nad}}[\rho_A,\rho_B](\mathbf{r})$, a short overview of the situation is given below. In the original and subsequent works by us and others, the bi-functional $T_s^{\mathrm{nad}}[\rho_A,\rho_B]$ (and the corresponding functional derivative—$v_t^{\mathrm{nad}}[\rho_A,\rho_B](\mathbf{r})$) was approximated by means of one of the known approximations for the functional $T_s[\rho]$.

$$\begin{aligned} T_s^{\mathrm{nad}}[\rho_A,\rho_B] &\approx \tilde{T}_s^{\mathrm{nad(decomposable)}}[\rho_A,\rho_B] \\ &= \tilde{T}_s[\rho_A+\rho_B]-\tilde{T}_s[\rho_A]-\tilde{T}_s[\rho_B] \end{aligned} \tag{5}$$

We refer to such approximations as "decomposable" for obvious reasons. In our original work on FDET [20], local-density approximation (Thomas–Fermi functional [56, 57]) and second-order [58] gradient expansion [59] for the kinetic energy was used to construct a decomposable approximation for the bi-functional $v_t^{\mathrm{nad}}[\rho_A,\rho_B](\mathbf{r})$. One of the surprising results reported in Ref. [20] was that the improvement in approximation to $T_s[\rho]$ by adding to the Thomas–Fermi functional the second-order gradient-expansion correction worsens the FDET interaction energies which are determined rather by the accuracy of the bifunctional $T_s^{\mathrm{nad}}[\rho_A,\rho_B]$. This observation was investigated further [60] showing that worsening the interaction energies can be attributed to the errors introduced into the potential $v_t^{\mathrm{nad}}[\rho_A,\rho_B](\mathbf{r})$. These observations lead us to the GGA97 bi-functional [61, 62], which is currently the most commonly used approximation for $T_s^{\mathrm{nad}}[\rho_A,\rho_B]$ in FDET-based numerical simulations. The GGA97 approximation for the bifunctional for $T_s^{\mathrm{nad}}[\rho_A,\rho_B]$ (and the corresponding $v_t^{\mathrm{nad}}[\rho_A,\rho_B](\mathbf{r})$) is obtained directly from the Lembarki–Chermette approximation for $T_s[\rho]$ [63]. In the Lembarki–Chermette approximation for $T_s[\rho]$, the second-order gradient-expansion contribution is attenuated locally depending on the magnitude of the reduced density gradient. This eliminates to some extent the errors in $v_t^{\mathrm{nad}}[\rho_A,\rho_B](\mathbf{r})$ originating in the second-order term in gradient-expansion approximation for $T_s[\rho]$. NDSD approximation (non-decomposable bi-functional using on up to second derivatives of density [64]) for $T_s^{\mathrm{nad}}[\rho_A,\rho_B]$, which does not have the decomposable form given in Eq. 5, is constructed to satisfy the exact asymptotic conditions for the bi-functional $v_t^{\mathrm{nad}}[\rho_A,\rho_B](\mathbf{r})$ of the greatest relevance near nuclear cusps. It has to be underlined that LDA, GGA97, and NDSD are all semi-local approximations for $T_s^{\mathrm{nad}}[\rho_A,\rho_B]$ (and the corresponding $v_t^{\mathrm{nad}}[\rho_A,\rho_B](\mathbf{r})$). At each point $\mathbf{r}$, the potential $v_t^{\mathrm{nad}}[\rho_A,\rho_B](\mathbf{r})$ is determined by the densities $\rho_A(\mathbf{r})$ and $\rho_B(\mathbf{r})$ and their first- and second derivatives at the same point. Such potentials were comprehensively shown to fail if the overlap between ρ_A and ρ_B is large [42, 60, 62, 65–67] as it is the case of an embedded subsystem covalently bound to the environment. For such cases an alternative strategy to approximate $v_t^{\mathrm{nad}}[\rho_A,\rho_B](\mathbf{r})$ is becoming increasingly popular which is based on numerical inversion of the Kohn–Sham potential [32, 33, 68, 69]. This work does not deal with such methods and aims at obtaining the exact properties based on semi-local approximation to $T_s^{\mathrm{nad}}[\rho_A,\rho_B]$, which are known to be applicable in case where the embedded subsystem is not covalently bound to the environment.

1.2 Interpretation of the electronic polarization of the environment in Frozen-Density Embedding Theory

Let us consider two choices for ρ_B : $\rho_B^{(1)}$ and $\rho_B^{(2)}$. In such a case,

$$\begin{aligned} E_{\mathrm{emb}}[\rho_B^{(1)}] &= \min_{\rho_A\geq 0,\ \int\rho_A(\mathbf{r})\mathrm{d}\mathbf{r}=N_A} E_v^{\mathrm{HK}}[\rho_A+\rho_B^{(1)}] \\ &= E_v^{\mathrm{HK}}[\rho_{A(\mathrm{opt})}^{(1)}+\rho_B^{(1)}] \end{aligned} \tag{6}$$

$$\begin{aligned} E_{\mathrm{emb}}[\rho_B^{(2)}] &= \min_{\rho_A\geq 0,\ \int\rho_A(\mathbf{r})\mathrm{d}\mathbf{r}=N_A} E_v^{\mathrm{HK}}[\rho_A+\rho_B^{(2)}] \\ &= E_v^{\mathrm{HK}}[\rho_{A(\mathrm{opt})}^{(2)}+\rho_B^{(2)}] \end{aligned} \tag{7}$$

where $\rho_{A(\mathrm{opt})}^{(1)}$ and $\rho_{A(\mathrm{opt})}^{(2)}$ are the optimized densities of subsystem A obtained for these two choices for ρ_B. On the virtue of the first Hohenberg–Kohn theorem [48], $E_{\mathrm{emb}}[\rho_B^{(1)}]=E_{\mathrm{emb}}[\rho_B^{(2)}]$ if $\rho_{A(\mathrm{opt})}^{(1)}+\rho_B^{(1)}=\rho_{A(\mathrm{opt})}^{(2)}+\rho_B^{(2)}$. Such situation is not uncommon. Let us consider $\rho_B^{(1)}$ and $\rho_B^{(2)}$ chosen in such a way that $\rho_B^{(1)}\leq\rho_{\mathrm{tot}}$ and $\rho_B^{(2)}\leq\rho_{\mathrm{tot}}$, where ρ_{tot} is the ground-state density of the whole system. Either Eq. 6 or 7 lead to the same total density (actually it is a ground-state density because the constraint $\rho\geq\rho_B$ is automatically satisfied for the chosen $\rho_B^{(1)}$ and $\rho_B^{(2)}$). The difference $\rho_B^{(1)}-\rho_B^o$, where ρ_B^o is the density of the isolated subsystem B, represents the electronic polarization of subsystem B due to interactions with subsystem A. But

since $\rho_B^{(1)}$ and $\rho_B^{(2)}$ are different, also $\rho_B^{(2)} - \rho_B^o$ differs from $\rho_B^{(1)} - \rho_B^o$! Despite the fact that they lead to the same total density, the two choices for ρ_B^o lead to different polarization (measured as the difference $\rho_B - \rho_B^o$). As a result, the term "electronic polarization of the environment" is not defined uniquely in FDET.

Even for such $\rho_B^{(1)}$ and $\rho_B^{(2)}$, for which $E_{\mathrm{emb}}[\rho_B^{(1)}]$ and $E_{\mathrm{emb}}[\rho_B^{(2)}]$ are not the same, the difference cannot be attributed only to different representation of electronic polarization of subsystem B. In FDET, it can originate from the fact that imposing the condition $\rho \geq \rho_B^{(1)}$ and $\rho \geq \rho_B^{(2)}$ involves different energy penalties, which is not directly related to the way the polarization is reflected in the choice for ρ_B. The same consideration apply for the interpretation of electronic polarization in subsystem A by switching the roles of A and B in the above considerations. The lack of unique definition of the "electronic polarization of the environment" in FDET makes FDET-based embedding methods different from empirical QM/MM type of approaches, in which the electronic polarization enters as a well defined contribution in the total energy expression which is frequently essential for accuracy (for a recent review see Ref. [5]).

The situation is quite different if approximate density functionals are used. We will discuss the differences in the case of subsystem densities optimized for both subsystems as it is made in Cortona's formulation of DFT [70]:

$$E_o = \min_{\substack{\rho_A \geq 0 \\ \int \rho_A(\mathbf{r})\mathrm{d}\mathbf{r}=N_A}} \min_{\substack{\rho_B \geq 0 \\ \int \rho_B(\mathbf{r})\mathrm{d}\mathbf{r}=N_B}} E_v^{\mathrm{HK}}[\rho_A + \rho_B] \tag{8}$$

The possibility of existence of several pairs yielding the same total energy has been long recognized [21, 71]. The same concerns FDET, where ρ_A is optimized whereas ρ_B is not. The analytical examples of such pairs are provided in Refs. [66, 71–73] whereas numerical examples for molecular systems are provided in Ref. [74]. It is useful to point out here the partition DFT formalism [49, 50], which can be seen as generalization of Cortona's subsystem DFT [70] allowing for a unique partitioning based on chemically motivated additional constraints.

If, however, approximations are used (denoted by tildes in the formulas below), the search given in Eq. 8 is not performed (see also the detailed discussion of this issue given by Gritsenko in Ref. [75]). Instead, another functional is minimized:

$$\tilde{E}_o = \min_{\substack{\rho_A \geq 0 \\ \int \rho_A(\mathbf{r})\mathrm{d}\mathbf{r}=N_A}} \min_{\substack{\rho_B \geq 0 \\ \int \rho_B(\mathbf{r})\mathrm{d}\mathbf{r}=N_B}} \left(E_v^{\mathrm{HK}}[\rho_A + \rho_B] + \Delta\tilde{E}_{\mathrm{xc}}[\rho_A + \rho_B] + \Delta\tilde{T}_s^{\mathrm{nad}}[\rho_A, \rho_B]\right) \tag{9}$$

where Δ denotes the error of a given functional (the difference between the exact functional and its approximated counterpart). Among all possible pairs yielding the same total electron density, the above search picks up that pair $\tilde{\rho}_A^{\mathrm{opt}}$ and $\tilde{\rho}_B^{\mathrm{opt}}$ which minimizes the error $(\Delta\tilde{T}_s^{\mathrm{nad}}[\rho_A, \rho_B])$ in the used approximation to the non-additive kinetic energy. The partitioning is thus unphysical. Note that the use of approximations into the exchange-correlation density functional cannot lead to uniqueness of partitioning because this energy component (and its errors) depends on the total density regardless how it is decomposed. The numerical practice using the *freeze-and-thaw* procedure [65] to perform minimization given in Eq. 9 shows that the use of $\tilde{T}_s^{\mathrm{nad}}[\rho_A, \rho_B]$ instead of $T_s^{\mathrm{nad}}[\rho_A, \rho_B]$ leads to a unique partitioning (for the overview see the articles quoted in Ref. [21]). In contrast with the situation in the formal framework of partition DFT [49, 50], partitioning obtained from Eq. 9 is unphysical.

If an approximation is used for $T_s^{\mathrm{nad}}[\rho_A, \rho_B]$, ρ_B which is optimized in the *freeze-and-thaw* procedure [65], the unique optimized ρ_B might differ from the density of the isolated subsystem B not only due to electronic polarization but also to the error on the non-additive kinetic potential. This error might result in artificial charge-redistribution between subsystems or qualitatively wrong polarization of subsystems [41, 60, 64, 76]. For this reason, we make a distinction between "polarization of subsystem B due to interactions with subsystem A" and "variational relaxation of subsystem B" in subsystem DFT calculations. The latter includes both the physical effect and the effect due to the error in the approximation used for the non-additive kinetic potential. The numerical importance of the two effects cannot be distinguished in practice. Based on our numerical experience, we believe that the error in currently used approximations for the non-additive kinetic potential affects the ρ_B optimized in the *freeze-and-thaw* procedure [65] more than neglecting the electronic polarization in the case of non-charged subsystem A non-covalently linked to subsystem B. The situation is different if subsystem A is charged. In such a case the relaxation can be attributed mainly to the electronic polarization (see also the discussion in the following section).

1.3 Previous studies of the dependence of molecular properties derived from FDET-based calculations on the choice for ρ_B

There are a practically infinite number of strategies to generate ρ_B in any multi-scale simulations based on FDET. They can be made based on "chemical intuition" or on dedicated tests made for model systems. In the previous section, the possible pitfalls associated with the notion of electronic polarization were identified on the formal grounds. The most straightforward strategy to generate ρ_B

is to use ground-state density obtained with some (usually less expensive) quantum mechanical method applied for the environment. Such calculations can be made in the absence of the embedded species or can take into effect the modification of the electron density of the environment by interactions with the embedded species. Numerical examples reported in the literature show frequently that optimizing the environment electron density (ρ_B) by means of the *freeze-and-thaw* cycle does not improve the calculated properties of non-charged embedded species. In the case of chromophores hydrogen bonded to the molecules in the environment, relaxing ρ_B results in the relative change of the excitation energy shift which does not exceed 25 % (the worst detected case) [37, 47, 77]. Moreover, the FDET hydrogen-bonding-induced shifts evaluated with non-relaxed ρ_B agree very well (i.e., within 200 cm^{-1} or better) with high-level wavefunction-based benchmark values [47, 77]. This suggests that the change in ρ_B following the "freeze-and-thaw" energy minimization is rather an effect due to the error in the bi-functional for the non-additive kinetic potential than to the physical effect of the polarization of the environment by the chromophore (see the discussion in the introduction section).

The use of non-relaxed ρ_B is, therefore, expected to be an adequate approximation for this type of weak interactions with the environment. Some properties are insignificantly affected by the relaxation of ρ_B even for charged embedded species. The shifts of the isotropic component of the hyperfine tensor A_{iso} of Mg^+ cation due to embedding in the noble gas matrix, evaluated for the *freeze-and-thaw* optimized and non-optimized ρ_B differ by less than 10 % [34]. This indicates that the effect of the noble gas matrix on the hyperfine tensor of embedded Mg^+ cation originates from the intermolecular Pauli repulsion (confinement effect) rather than from the electric polarization of the matrix by the cation. Concerning the notion of "polarization of the environment", there are cases where it might be helpful in constructing a good approximation for ρ_B such as a highly charged species embedded in highly polarizable environment. The ligand-field splitting of *f*-levels for a trivalent rare-earth cation impurity in a host lattice (chloroelpasolite) might be considered as an extreme example. The nearest ligands of the impurity are Cl^- anions and the use of non-relaxed ρ_B to represent the six ligands seems a very crude approximation in FDET calculations. Indeed, only the qualitative trends for the ligand-field splitting parameters along the lanthanide series are reproduced using non-relaxed ρ_B in KSCED calculations [36]. The FDET splittings calculated at non-relaxed ρ_B are, however, underestimated by a factor of about two. The use of *freeze-and-thaw* optimized ρ_B results in about twofold increase of the splittings, which brings them close to experimental values. Ref. [36] shows also how the rather expensive *freeze-and-thaw* calculations can be avoided even in such extreme case (highly charged subsystem *A* and highly polarisable subsystem *B*) by means of "pre-polarized" ρ_B. Generating the "pre-polarized" ρ_B is quantitatively less expensive than the *freeze-and-thaw* relaxation because it involves just a simple calculation of the ligands in the electric field generated by the embedded cation. The splittings obtained using *freeze-and-thaw* optimized ρ_B and "pre-polarized" ρ_B are almost the same (they agree within 10 cm^{-1}).

The above examples taken from the literature indicate that the choice of ρ_B in FDET-based calculations is the issue calling for a special attention especially since the notion of "polarization" and "relaxation" are not equivalent in FDET as discussed in the previous section. It is a crucial issue in multi-level simulations in which ρ_B represents a system of significantly larger size than subsystem *A* for which quantum mechanical descriptors (orbitals or the non-interacting reference system [20, 21], embedded interacting wavefunction [22], or one-particle reduced density matrix [23]) are constructed. It is, therefore, desirable that generation of an adequate ρ_B involves smaller computational costs than the optimization of ρ_A and the subsequent evaluation of quantum mechanical observables for subsystem *A*. Even in the cases, for which avoiding the optimization of ρ_B is an acceptable approximation, it is highly desirable to use a protocol to generate ρ_B which involves the smallest computational effort. The aim of the present work is a systematic analysis of strengths and weaknesses of possible practical strategies to generate non-relaxed ρ_B for FDET calculations for chromophores in hydrogen-bonded molecular environments.

2 Computational details

2.1 Strategies to generate the frozen electron density—ρ_B

For each considered system, the excitation energies are evaluated using densities of the environment (ρ_B) obtained by means of different computational techniques. The approximations and technical parameters concerning subsystem *A* remain, however, unchanged: (1) approximations for $E_{xc}[\rho_A]$, $T_s^{nad}[\rho_A, \rho_B]$, and $E_{xc}^{nad}[\rho_A, \rho_B]$; (2) atomic basis set used for subsystem *A*; and (3) parameters of technical nature (grids, fitting functions, convergence criteria, etc.) as in the reference calculations. This approach provides direct information concerning the dependence of the FDET calculated excitation energies on ρ_B.

The following simplified methods to generate ρ_B are considered:

(A) *Superposition of atomic densities*

The simplest approximation for the electron density of the environment ρ_B is to use a superposition of atomic densities.

$$\rho_B(\mathbf{r}) = \sum_{i=1}^{N\text{atom}B} (n_B^i - Z_B^i)\rho_B^i(\mathbf{r}) \tag{10}$$

where i indicates the atom in subsystem B, Natom$B$ is the number of atoms in subsystem B, $\rho_B^i(\mathbf{r})$ denotes the spherically symmetric electron density integrating to the total charge equal to the atomic number Z_B^i, and n_B^i denotes the net charge of the atom. The above approximation for ρ_B can be expected to take into account Pauli repulsion between electrons, which are localized in closed shells of atoms in the environment, and the electrons in subsystem A even if $\{n_B^i = 0\}$ (electrically neutral atoms in the environment). In the case when the effect of the environment on the electronic structure is dominated by confinement, choosing $\{n_B^i = 0\}$ can be expected an adequate approximation. For a polar or charged molecule in the environment, taking $\{n_B^i = 0\}$ is most likely a very poor approximation because it would neglect the dominant (i.e. electrostatic) term in the FDET embedding potential at long range. The choice of n_B^i becomes, in such case, the key issue. This approximation for ρ_B was already applied for chromophores in ionic solids [38]. In such a case, a natural choice for n_B^i, is to use the formal ionic charges. Indeed, the numerical tests made for fluorenone embedded in zeolite L reported in Ref. [38] confirm the adequacy of the approximation given in Eq. 10 in the case of the environment being an ionic solid.

(B) *Superposition of molecular densities*

Approximating $\rho_B(\mathbf{r})$ by means of a sum of molecular densities seems to be a particularly appealing strategy if the environment consists of many weakly interacting molecules. In such a case, $\rho_B(\mathbf{r})$ is obtained as:

$$\rho_B(\mathbf{r}) = \sum_{i=1}^{N\text{molec}B} \rho_B^i(\mathbf{r}) \tag{11}$$

where Nmolec$B$ is the number of molecules in subsystem B, $\rho_B^i(\mathbf{r})$ denotes the electron density of the isolated ith molecule.

Approximation given in Eq. 11 was used in the first multi-scale simulations based on FDET concerning ground-state properties of solvated molecules [78, 79]. The adequacy of this approximation for simulating the hydrogen transfer reaction in carbonic anhydrase was investigated in Ref. [35].

Increasing the strength of the interactions between the molecules in subsystem B might invalidate the approximation given in Eq. 11. In the present work, the applicability of Eq. 11 to molecular environment is investigated using complexes of *cis*-7-hydroxyquinoline and several molecules which are hydrogen bonded to the chromophore but also interact via hydrogen bonds among themselves. If the molecules in the environment form a hydrogen-bonded chain, the mutual polarization of the neighboring molecules in the chain, leads to non-additive increase of the total dipole moment. The obtained results can, therefore, be considered as good estimate of maximum error made due to the neglect of such cooperative effects in hydrogen-bonded molecular environments. The presence of hydrogen-bonded chains of molecules in the environment is the "worst scenario" as far as applicability of Eq. 11 is concerned.

(C) *Less expensive Kohn–Sham calculations for the whole environment*

In practice, it is appealing to use less expensive approximations to solve Kohn–Sham equations for the entire environment (subsystem B) than for subsystem A. In contrast with the approximations given in Eqs. 10 and 11, mutual polarization of molecules in the environment is taken into account.

2.2 Miscellaneous computational details

All reported results are obtained using the ADF code [80] into which the ground-state and linear-response time-dependent excited-state FDET calculations were implemented as described in Refs. [37, 81] with subsequent improvements described in detail in Refs. [82]. Slater type orbitals (STO) [83] are used for both subsystems (A and B). Unless specified otherwise, STO–aug-TZP basis set is used for the embedded subsystem (subsystem A). The use of diffuse functions for subsystem A increases the sensibility of the FDET results in change of the embedding potential which might occur as a consequence of changes in ρ_B. For ρ_B or for its components, the basis sets are ranging from STO–SZ to STO–aug-TZ2P and they are specified in each case. The following approximations for density (or orbital) functionals are used: (1) SAOP [84, 85] for $v_{\text{xc}}[\rho_A](\mathbf{r})$, i.e., the exchange-correlation potential in subsystem A, (2) the decomposable approximation using the PW91 [86] exchange-correlation functional for $v_{\text{xc}}^{\text{nad}}[\rho_A, \rho_B](\mathbf{r})$, i.e., the non-additive exchange-correlation bi-functional in Eq. 3, (3) either NDSD functional [64] or the decomposable approximation GGA97 [61] obtained from the Lembarki–Chermette functional for the kinetic energy [63] for $v_t^{\text{nad}}[\rho_A, \rho_B](\mathbf{r})$, the non-additive kinetic potential in Eq. 3. In the case of other approximations, they are specified in the relevant part of the "Results" section. The technical

parameters used in the present study are not optimized for speed of calculations but are set up to eliminate or to keep constant other factors (than the choice for ρ_B), which affect the FDET results. In particular, the exchange-correlation- and the non-additive components of the embedding potential are evaluated at "exact" densities, i.e., electron densities evaluated from orbitals without the use of fitting functions.

3 Results

This section comprises two parts. The first one concerns the same chromophore—*cis*-7-hydroxyquinoline—in environments comprising up to three hydrogen-bonded molecules. The three strategies to generate ρ_B are applied and the corresponding environment-induced shifts of the $\pi \rightarrow \pi^*$ excitation energies are discussed in order to select the most robust strategy to generate ρ_B in large-scale multi-level simulations for similar chromophores in soft condensed matter. In the second part, the most robust strategy (Kohn–Sham calculations for the whole environment) is applied for larger environments of other chromophores in order to verify the applicability of this strategy.

3.1 *cis*-7-Hydroxyquinoline in hydrogen-bonded complexes

These systems are ideal objects for studying the dependence of the calculated complexation induced shifts of the excitation energy on the choice made for ρ_B in FDET/LR-TDDFT calculations. The studied excitations are local. They fall, therefore, in the domain of applicability of FDET. The molecules do not absorb noticeably within the considered spectral range, which makes the NDRE approximation applicable. Moreover, benchmark quality excitation energies obtained from high-level wavefunction methods are available for the smallest of these complexes [47, 77]. It was shown that FDET calculations reproduce very accurately both the reference benchmark shifts of the excitation energy and the experimental shifts, provided ρ_B is obtained from Kohn–Sham calculations for the isolated environment [47, 77]. These FDET excitation energy shifts are used as a reference for the present work in which ρ_B is generated by means of alternative (simpler) methods. The geometries of the considered "microsolvated" *cis*-7-hydroxyquinoline clusters are also taken from Refs. [47, 87].

3.1.1 *Superposition of atomic densities for the environment*

The applicability of approximation given in Eq. 10 is studied for the complexes *cis*-7-hydroxyquinoline-H_2O and *cis*-7-hydroxyquinoline-NH_3. In the considered complexes, the search of the optimal n_B^i is especially straightforward because once the net atomic charge on the non-hydrogen atom is fixed, the charges on hydrogens are uniquely determined by the condition of neutrality of the whole molecule ($n_B^{\mathrm{H}} = -n_B^{\mathrm{O}}/2$ for H_2O and $n_B^{\mathrm{H}} = -n_B^{\mathrm{N}}/3$ for NH_3). The search for the optimal n_B^i can be performed, therefore, in one dimension by varying the net charge on non-hydrogen atom from 0 (neutral atom) to -1 e (complete charge transfer from hydrogens). The principal orbitals contributing to the lowest excitation are shown in Fig. 1.

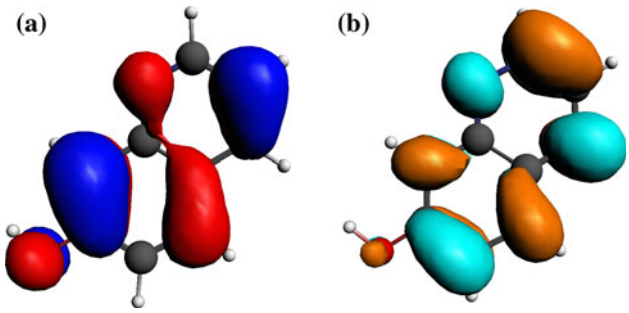

Fig. 1 The pair of molecular orbitals in isolated *cis*-7-hydroxyquinoline, which provides the dominant contribution to the lowest excitation (HOMO on the *left side* and LUMO on the *right side*)

Figures 2 and 3 show the excitation energy shifts calculated for the considered range of atomic net charges. The shifts depend critically on the chosen values of n_B^i in Eq. 10 in both complexes. The increase of the polarity of the molecule in the environment increases also the magnitude of the red shift. The benchmark results for the 7HQ + H_2O complex are reproduced at the net charge at oxygen of about -0.7 e. Interestingly, the oxygen net charge obtained from the Mulliken population analysis lies within this range. The use of any other common methods to decompose the molecular charge into atomic contributions leads to slightly worse shifts but seems also to be a reasonable choice.

Unfortunately, none of the common methods to obtain the net charges in ammonia seems to be useful to generate ρ_B by means of Eq. 10. The best agreement with the reference values for the shift occurs for $n_B^{\mathrm{N}} < -1.0$ e. None of the standard methods to partition the molecular electron density into atomic contributions considered here leads to such a value of the net charge. Similar conclusions can be drawn using smaller basis sets for subsystem A such as STO–DZP, STO–TZP (data available from the authors upon request). Most likely, using the spherical atomic charges is too crude as an approximation to represent properly the electric field generated by the lone pair of nitrogen. A universal procedure to generate net atomic charges to be used in Eq. 10 is hardly in view. Obtaining

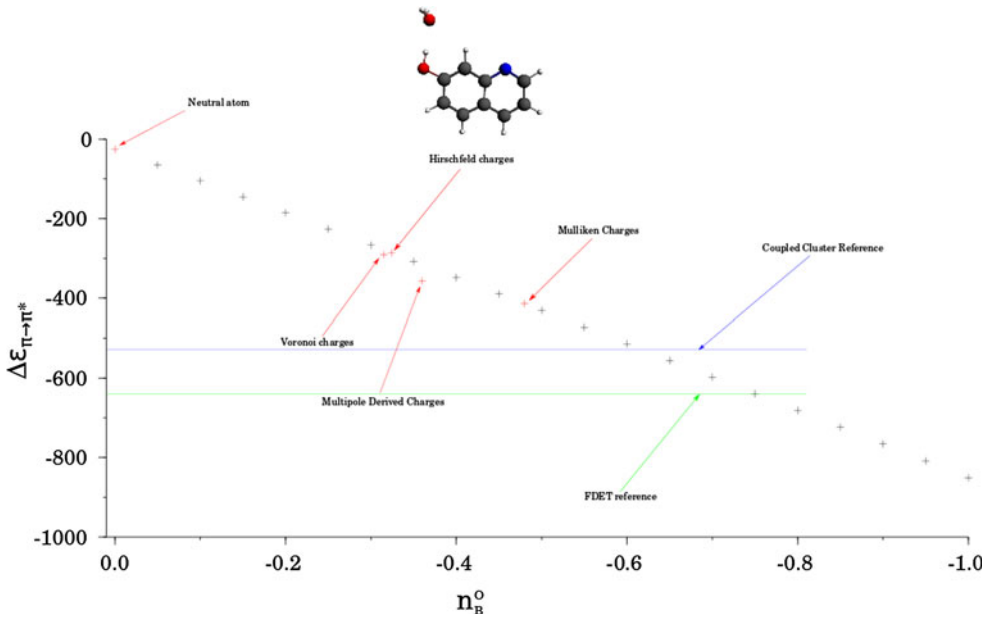

Fig. 2 Dependence of the complexation induced shift (in cm^{-1}) of the lowest $\pi \to \pi^*$ excitation in the complex of *cis*-7-hydroxyquinoline with water on the net atomic charges used in Eq. 10 for generating the frozen density $\rho_B = \rho_{H_2O} \cdot n_B^O$ is the net charge on oxygen and the charge on each hydrogen equals to $-n_B^O/2$. The wavefunction and FDET reference values taken from Ref. [47] are indicated as *horizontal lines*. Results obtained using common methods for generating net atomic charges: Mulliken population analysis [88], Hirschfeld population analysis [89], Voronoi charges [90], multipole derived [91] are also indicated. STO–DZP basis set is used for generation of ρ_B

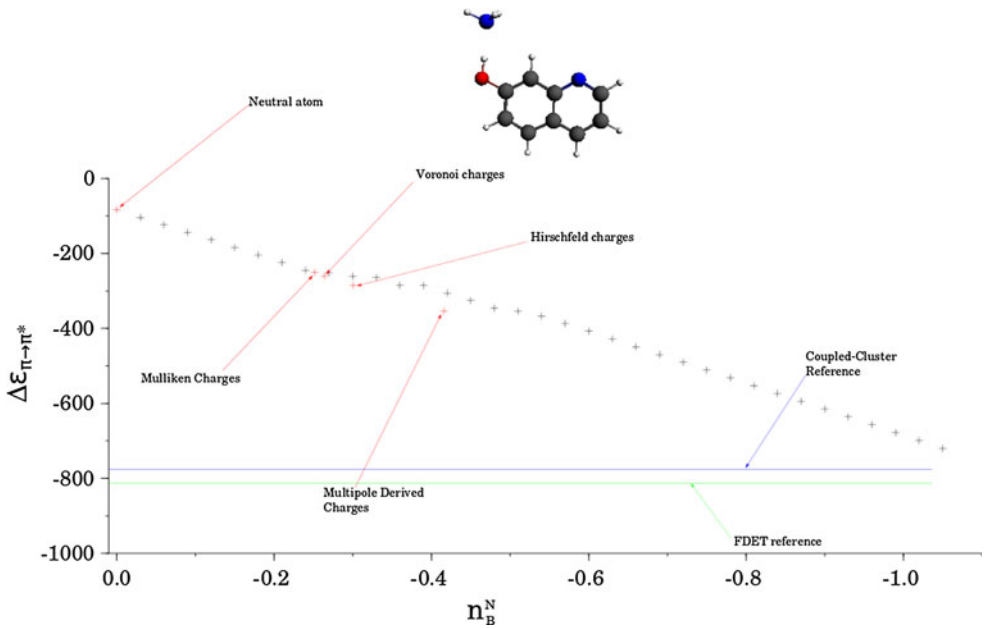

Fig. 3 Dependence of the complexation induced shift (in cm^{-1}) of the lowest $\pi \to \pi^*$ excitation in the complex of *cis*-7-hydroxyquinoline with ammonia on the net atomic charges used in Eq. 10 for generating the frozen density $\rho_B = \rho_{NH_3} \cdot n_B^N$ is the net charge on nitrogen and the charge on each hydrogen equals to $-n_B^N/3$. The wavefunction and FDET reference values taken from Ref. [47] are indicated as *horizontal lines*. Results obtained using common methods for generating net atomic charges: Mulliken population analysis [88], Hirschfeld population analysis [89], Voronoi charges [90], multipole derived [91] are also indicated. STO–DZP basis set is used for generation of ρ_B

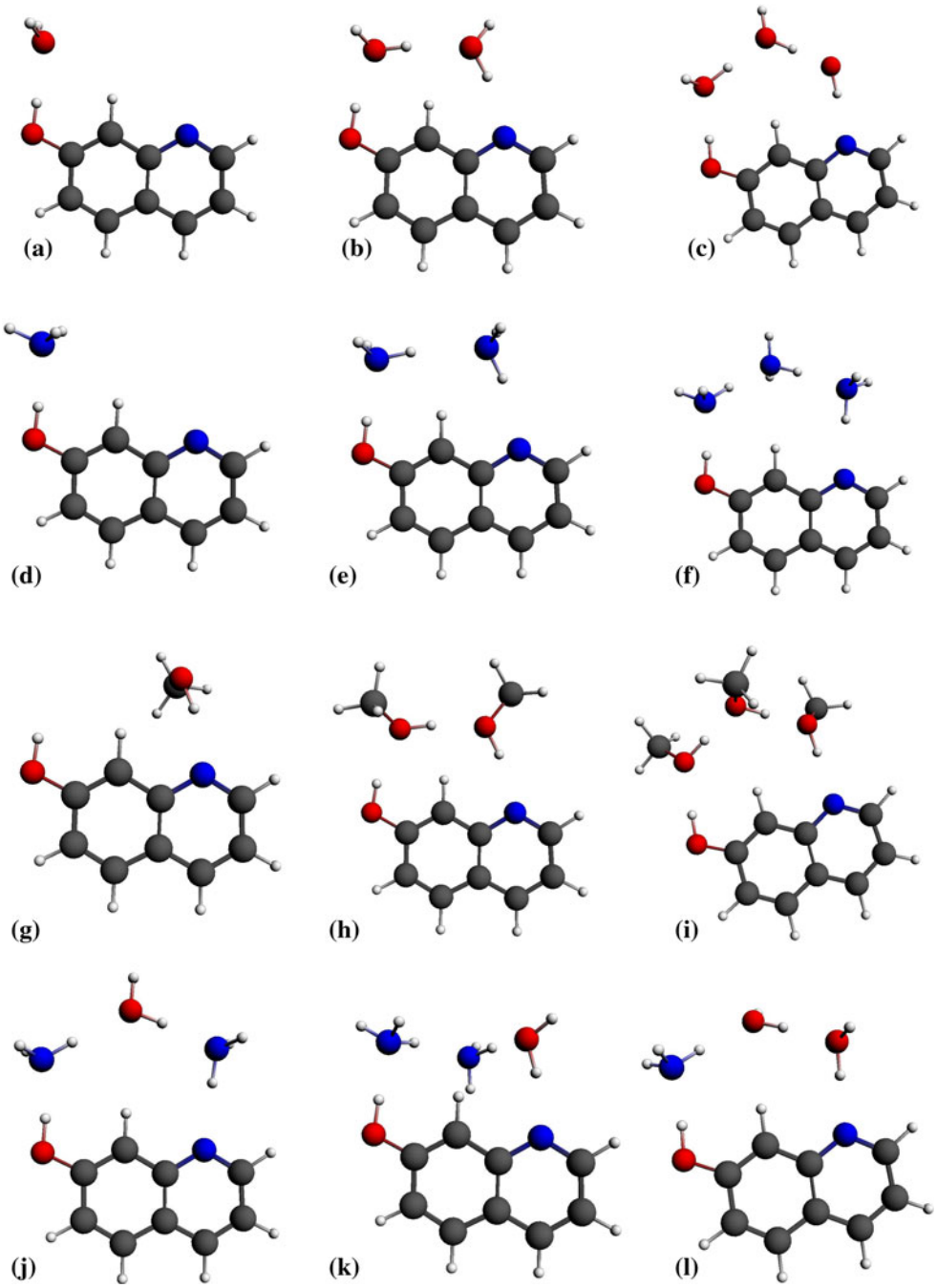

Fig. 4 *cis*-7-Hydroxyquinoline (7HQ) in complexes investigated in this work: **a** 7HQ–H_2O, **b** 7HQ–$2H_2O$, **c** 7HQ–$3H_2O$, **d** 7HQ–NH_3, **e** 7HQ–$2NH_3$, **f** 7HQ–$3NH_3$, **g** 7HQ–CH_3OH, **h** 7HQ–$2CH_3OH$, **i** 7HQ–$3CH_3OH$, **j** 7HQ–NH_3–H_2O–NH_3, **k** 7HQ–NH_3–NH_3–H_2O, **l** 7HQ–NH_3–H_2O–H_2O

ρ_B from Eq. 10 is, therefore, not practical for environments comprising polar molecules despite its usefulness in the case of ionic solids [38].

Turning back to the dependence of the shift on the net charge, we notice that the calculated shifts are very small (a few cm^{-1} for 7HQ + NH_2O and less than 100 cm^{-1} for 7HQ + NH_3) at the neutral atom limit ($n_B^i = 0$) at which the long-range electrostatic component of the embedding potential disappears. This indicates that confinement is a minor factor determining the shifts. The non-electrostatic components of the embedding potentials are present regardless of which value of the net atomic charge is used whereas the electrostatic component is proportional to the magnitude of the net atomic charges (see Eqs. 3, 10). It is also worthwhile noticing the almost linear dependence of the shifts on the net charge supporting the electrostatic interpretation of the origin of the shift.

3.1.2 *Superposition of molecular densities*

The results obtained in the previous section indicate that the simplest strategy (superposition of atomic densities)

Table 1 Environment-induced shifts ($\Delta\varepsilon_{\pi-\pi^*}$) of the lowest $\pi \rightarrow \pi^*$ excitation energy for *cis*-7-hydroxyquinoline in various environments evaluated using either the reference ρ_B (Kohn–Sham calculations for the whole environment) or ρ_B obtained as superposition of molecular densities (Eq. 11). The differences between the excitation energies obtained at these two choices for ρ_B ($\varepsilon[\rho_B^{\text{Eq.11}}] - \varepsilon[\rho_B^{\text{KS}}]$) are given in parentheses. STO–aug-TZ2P basis set is used for ρ_A generation. STO–DZP basis set is used for ρ_B generation

Choice for ρ_B	Environment					
	$\Delta\varepsilon_{\pi-\pi^*}$ (cm^{-1})					
	$2H_2O$	$3H_2O$	$2NH_3$	$3NH_3$	$2CH_3OH$	$3CH_3OH$
$\rho_B = \rho_B^{\text{Eq.11}}$	−1493	−1176	−1158	−1154	−1309	−1275
$\rho_B = \rho_B^{\text{KS}}$	−1614	−1545	−1225	−1392	−1450	−1625
	(121)	(369)	(67)	(238)	(141)	(350)

Table 2 Environment-induced shifts ($\Delta\varepsilon_{\pi-\pi^*}$) of the lowest $\pi \rightarrow \pi^*$ excitation energy for *cis*-7-hydroxyquinoline in various environments evaluated using either the reference ρ_B (Kohn–Sham calculations for the whole environment) or ρ_B obtained as superposition of molecular densities (Eq. 11). The differences between the excitation energies obtained at these two choices for ρ_B ($\varepsilon[\rho_B^{\text{Eq.11}}] - \varepsilon[\rho_B^{\text{KS}}]$) are given in parentheses. STO–aug-TZ2P basis set is used for ρ_A generation. STO–DZP basis set is used for ρ_B generation

Choice for ρ_B	Environment		
	$\Delta\varepsilon_{\pi-\pi^*}$ (cm^{-1})		
	NH_3–H_2O–NH_3	NH_3–NH_3–H_2O	NH_3–H_2O–H_2O
$\rho_B = \rho_B^{\text{Eq.11}}$	−1483	−1716	−1636
$\rho_B = \rho_B^{\text{KS}}$	−1735	−1817	−1856
	(252)	(101)	(220)

Table 3 Environment-induced shifts ($\Delta\varepsilon_{\pi-\pi^*}$) of the lowest $\pi \rightarrow \pi^*$ excitation energy for *cis*-7-hydroxyquinoline environments comprising broken-hydrogen chains evaluated using either the reference ρ_B (Kohn–Sham calculations for the whole environment) or ρ_B obtained as superposition of molecular densities (Eq. 11). The differences between the excitation energies obtained at these two choices for ρ_B ($\varepsilon[\rho_B^{\text{Eq.11}}] - \varepsilon[\rho_B^{\text{KS}}]$) are given in parentheses. STO–aug-TZ2P basis set is used for ρ_A generation. STO–DZP basis set is used for ρ_B generation

Choice for ρ_B	Environment		
	$\Delta\varepsilon_{\pi-\pi^*}$ (cm^{-1})		
	$2H_2O$	$2NH_3$	$2CH_3OH$
$\rho_B = \rho_B^{\text{KS}}$	−899	−900	−1010
$\rho_B = \rho_B^{\text{Eq.11}}$	−881	−888	−993
	(17)	(12)	(18)

might lead to erratic FDET shifts if the environment is a polar molecule. The results are very sensitive to the arbitrary choice of the procedure to generate net atomic charges. As the ammonia example shows, it might even not be possible to generate appropriate net charges.

For environments consisting of several polar molecules the second strategy (Eq. 11) appears as the only option. It is investigated for complexes comprising *cis*-7-hydroxyquinoline embedded in such environments as: $2H_2O$, $3H_2O$, $2NH_3$, $3NH_3$, $2CH_3OH$, and $3CH_3OH$. The complexes are shown in Fig. 4. The geometries of these complexes are taken from Refs. [47, 87], which provide also reference benchmark shifts from EOM-CC and FDET calculations. The chosen systems represent well the worst scenario as far as the approximation introduced in Eq. 11 is concerned. In each case, the molecules in the environment form chain-like structures (see Fig. 4) and the effect of mutual polarization can be expected to be large. Indeed, according to our own studies reported in Ref. [8], this mutual polarization lies at the origin of the positive cooperativity in the solvatochromic shift if the hydrogen-bonded chains consists of more than two hydrogen-bonded molecules.

Using ρ_B as the superposition of electron densities of isolated individual molecules from the environment instead of the Kohn–Sham density obtained for the whole environment affects the shifts noticeably—from 67 cm^{-1} in the case of two ammonia molecules to as much as 369 cm^{-1} in the case of three water molecules forming a chain (see Tables 1, 2). The relative errors in the shifts due to the approximation given in Eq. 11 can reach up to 25 % (the case of three membered chains). Therefore, it can not be considered as a generally adequate approximation.

However, in some cases, generating ρ_B using Eq. 11 is an acceptable approximation. The following computational experiment concerns such a case. The shifts are calculated for the longest chains (three molecules in the environment) but with the central molecule removed to break the chain. The mutual polarization of the molecules in the environment is reduced as the result. As expected, the differences between shifts obtained using superposition of molecular densities and densities derived from Kohn–Sham

Table 4 Environment-induced shifts ($\Delta\varepsilon_{\pi-\pi^*}$) of the lowest $\pi \rightarrow \pi^*$ excitation energy for *cis*-7-hydroxyquinoline environments comprising broken-hydrogen chains evaluated using either the reference ρ_B (Kohn–Sham calculations for the whole environment) or ρ_B obtained as superposition of molecular densities (Eq. 11). The differences between the excitation energies obtained at these two choices for ρ_B ($\varepsilon[\rho_B^{\text{Eq.11}}] - \varepsilon[\rho_B^{\text{KS}}]$) are given in parentheses. STO–aug-TZ2P basis set is used for ρ_A generation. STO–DZP basis set is used for ρ_B generation

Choice for ρ_B	Environment		
	$\Delta\varepsilon_{\pi-\pi^*}$ (cm^{-1})		
	NH_3–NH_3	NH_3–H_2O	NH_3–H_2O
$\rho_B = \rho_B^{\text{KS}}$	−1172	−1545	−1309
$\rho_B = \rho_B^{\text{Eq.11}}$	−1161	−1529	−1297
	(11)	(16)	(12)

calculations for the whole environment are negligible (see Tables 3, 4).

The results indicate clearly that the computationally attractive strategy in which ρ_B is approximated as a sum of electron densities in the isolated molecules is a very good pragmatic solution for hydrogen-bonded clusters in the absence of direct hydrogen bonding between the molecules in the environment. Replacing one Kohn–Sham calculation for the whole environment by several less expensive calculations for each individual molecule in the environment affects the excitation energies by at the most 20 cm^{-1}. In the case of direct hydrogen bonding between the molecules in the environment, the errors due to neglect of mutual polarization between the molecules in the environment are significantly larger (up to 400 cm^{-1}). Such errors might be considered acceptable for some applications (they still do not exceed 25 % of the total shifts). If a better accuracy is needed and the presence of the hydrogen-bonded chains cannot be excluded, the mutual polarization of the molecules in the environment must be taken into account. The subsequent section concerns such a case.

Although the principal interest of the present work lies in the dependency of FDET excitation energies on ρ_B, Tables 10, 11, 12 and 13 in the Supporting Information collect also the excitation energy shifts obtained using other basis sets for subsystem *A*. The approximation given in Eq. 11 leads to the effect on the shifts which is practically independent on the basis set used for subsystem *A*. This justifies attributing the difference between the excitation energy obtained with Eq. 11 and with full Kohn–Sham treatment of subsystem *B* to a physical effect—mutual polarization of the molecules in the environment. Data collected in Tables 10 and 11 of Supporting Information demonstrate remarkable numerical stability of the shifts with respect to the changes of the basis set used for subsystem *A*. Upon changing the basis set for subsystem *A*, the shifts vary within about 20 cm^{-1}. Such small variation is negligible compared to the magnitude of the shifts, which are about one order of magnitude larger. This stability of the shifts reflects the variational origin of the FDET embedding potential and the adequacy of the used approximation for the non-additive kinetic potential.

3.1.3 Kohn–Sham calculations for the whole environment

As shown in the previous section, neglecting the mutual polarization of the molecules in the environment (approximation made in Eq. 11) leads to significant errors in the complexation induced shifts of excitation energy (up to 25 % of the total shift) if the molecules in the environment form longer hydrogen-bonded chains. The errors are not significant in the absence of such chains. This suggests that, in order to generate ρ_B in the case of modeling chromophores in hydrogen-bonded environments such as liquid water, the whole environment should be treated at the molecular orbital level of description. The chosen method should be inexpensive and take into account the mutual polarization of the molecules in the environment properly. Ground-state Kohn–Sham calculations for the whole environment can be, therefore, considered as a practical option. Depending on the choice of the functional and the basis set, such calculations lead to different ρ_B, which in turn leads to different dipole moment of the environment. In the present section, the effect of these choices on the calculated excitation energy shifts is investigated. For each among the five clusters 7HQ − $(H_2O)_n$ (for $n = 1$–3) and 7HQ − $(NH_3)_n$ (for $n = 1$–2) three series of ρ_B were generated by means of Kohn–Sham calculations for the whole environment. In each series, a different approximation for the exchange-correlation potential was used (LDA [92, 93], PBE [94], or SAOP [84, 85]) and the following slater type atomic basis sets: STO–SZ, STO–DZP, STO–TZP, STO–TZ2P, and STO–aug-TZP [83]. In all calculations, the same basis set was used for subsystem *A* (STO–aug-TZ2P) and the same approximation for the exchange-correlation energy of subsystem *A* (SAOP [84, 85]). Figure 5 shows that the complexation induced shifts are almost independent on the dipole moment of subsystem *B*.

The shifts show remarkable stability in each case. In the H_2O case, changing the basis set and the approximation for the exchange-correlation potential results in variation of the magnitude of the dipole moment from 1.77 to 1.94 Debye which is accompanied by a small variation of the excitation energy (from 3.7062 to 3.7123 eV). Since the excitation energy for the isolated chromophore is the same in each case (the same basis set and approximation for the exchange-correlation potential for subsystem *A*) the variation of the shifts is the same (they vary within 0.0061 eV).

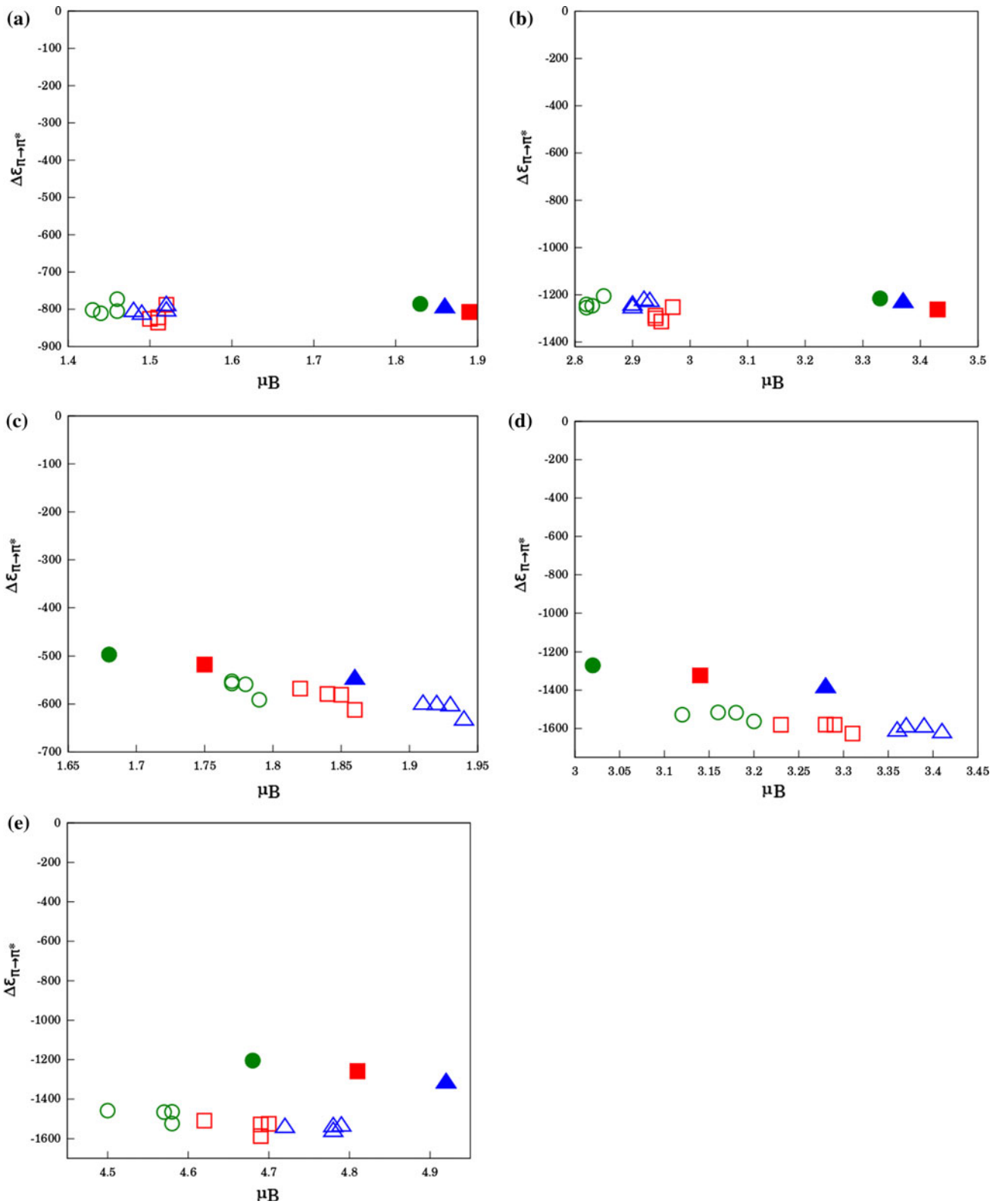

Fig. 5 Complexation induced shifts of the excitation energy ($\Delta\varepsilon_{\pi-\pi^*}$) in *cis*-7-hydroxyquinoline (7HQ) in hydrogen-bonded clusters evaluated at frozen densities (ρ_B) differing in the dipole moment (μ_B). ρ_B generated in Kohn–Sham calculations for isolated environment applying LDA (*squares*), PBE (*circles*), and SAOP (*triangles*) exchange-correlation potentials and basis sets ranging from STO–SZ to STO–aug-TZP): **a** 7HQ–NH_3, **b** 7HQ–$(NH_3)_2$, **c** 7HQ–H_2O, **d** 7HQ–$(H_2O)_2$, and **e** 7HQ–$(H_2O)_3$. The results obtained with minimal basis set (STO–SZ) are indicated with *full symbols*. The zero line, i.e., $\Delta\varepsilon = 0$, corresponds to the isolated chromophore, i.e., $v_{\text{emb}}[\rho_A, \rho_B, v_B](\mathbf{r}) = 0$

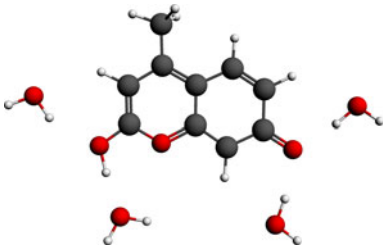

Fig. 6 The cluster of keto-7-hydroxy-4-methylcoumarin and four water molecules

The change of the dipole moment of the environment by 0.17 Debye (10 % relative change) is followed by the change of the excitation energy by 0.0061 eV (which is only 3 % of the shift). Calculations for other environments show a similar trend. Despite the fact that it is electrostatics, which provides the dominant contribution to the shifts, hardly any correlation between the dipole moment of the environment and the calculated shift in the excitation energy can be observed.

The results obtained for embedded *cis*-7-hydroxyquinoline suggest the optimal strategy to generate ρ_B consisting of using a low-end Kohn–Sham calculations for the whole isolated subsystem B which assures taking properly into account the mutual polarization of the molecules in the environment. Among the two factors determining the shifts: neglecting the mutual polarization of the molecules in the environment (the physical approximation) and the use of medium quality basis set (implementation related effect), the first one appears to be clearly more significant. In the following two sections, this recommendation is put to scrutiny using other hydrated chromophores.

3.2 Dependence of the environment-induced shifts of the excitation energies on ρ_B obtained from the Kohn–Sham calculations for the whole environment

In computational studies on solvatochromism, a large number of molecules of the solvent is explicitly included. The issue of inexpensive generation of ρ_B is critical for saving computation time. This section deals with the issue: *How far one can go in simplifying the Kohn–Sham calculations for the whole environment without deteriorating the FDET calculated shifts in the energies of local excitations?*

3.2.1 Microsolvated keto-7-hydroxy-4-methylcoumarin

The excited-state properties of keto-7-hydroxy-4-methylcoumarin (7H4MC) are widely studied experimentally and

Table 5 Excitation energies (ε) and environment-induced spectral shifts ($\Delta\varepsilon$) of the three lowest excitations obtained using different choices for ρ_B (Kohn–Sham calculations with three choices for exchange-correlation potentials and four choices for the basis sets) for the 7-hydroxy-4-methylcoumarin complex with four H_2O molecules. The corresponding excitation energy for isolated chromophore are: $\varepsilon_{\pi\to\pi^*(1)} = 2.9245$ eV, $\varepsilon_{\pi\to\pi^*(2)} = 4.4061$ eV, and $\varepsilon_{n\to\pi^*} = 2.7340$ eV. The corresponding dipole moment (in Debye units) of the environment is also given

Generation of ρ_B		Excitation Energy (eV)			Spectral shift (cm^{-1})			μ_B (Debye)
Xc-potential	Basis set	$\varepsilon_{\pi\to\pi^*(1)}$	$\varepsilon_{\pi\to\pi^*(2)}$	$\varepsilon_{n\to\pi^*}$	$\Delta\varepsilon_{\pi\to\pi^*(1)}$	$\Delta\varepsilon_{\pi\to\pi^*(2)}$	$\Delta\varepsilon_{n\to\pi^*}$	
SAOP	STO–SZ	2.7376	4.4058	3.3832	−1507	−2	5236	5.23
	STO–DZ	2.9824	3.4543	3.7178	466	−462	5810	7.62
	STO–DZP	3.0243	4.5178	3.4349	805	901	5653	5.44
	STO–TZP	3.0155	4.5113	3.4232	734	848	5559	5.39
	STO–TZ2P	3.0233	4.5168	3.4196	797	893	5530	5.42
	STO–aug-TZP	3.0241	4.5118	3.4184	803	852	5520	5.25
PBE	STO–SZ	2.8288	4.4252	3.3404	−772	154	4891	4.68
	STO–DZ	3.0106	3.7320	3.4047	694	−384	5410	7.09
	STO–DZP	3.0206	4.5109	3.4003	775	845	5374	4.94
	STO–TZP	3.0066	4.5004	3.3880	662	761	5275	4.99
	STO–TZ2P	2.9935	4.4993	3.3822	556	751	5228	5.03
	STO–aug-TZP	3.0119	4.4992	3.3712	705	751	5139	5.06
LDA	STO–SZ	2.9231	4.4632	3.3585	−11	460	5037	4.94
	STO–DZ	3.0086	3.4250	3.7256	677	−399	5573	7.50
	STO–DZP	3.0167	4.5142	3.4081	744	872	5437	5.13
	STO–TZP	3.0183	4.5111	3.3986	793	847	5360	5.19
	STO–TZ2P	3.0185	4.5114	3.3935	758	849	5319	5.22
	STO–aug-TZP	3.0152	4.5087	3.3838	732	827	5241	5.25

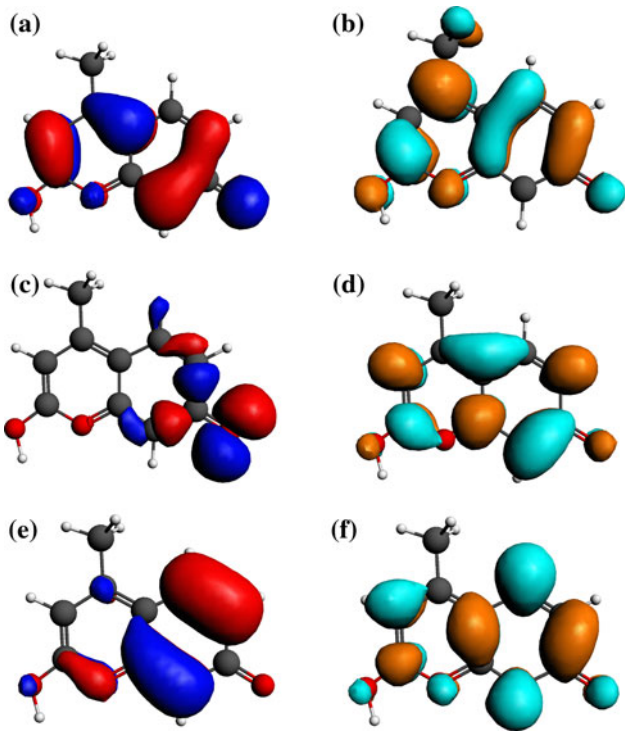

Fig. 7 The molecular orbitals in isolated keto-7-hydroxy-4-methyl-coumarin, which provide the dominant contributions to the lowest excitations: **a** HOMO, **b** LUMO, **c** HOMO−1, **d** LUMO+1, **e** HOMO−2, and **f** LUMO+2

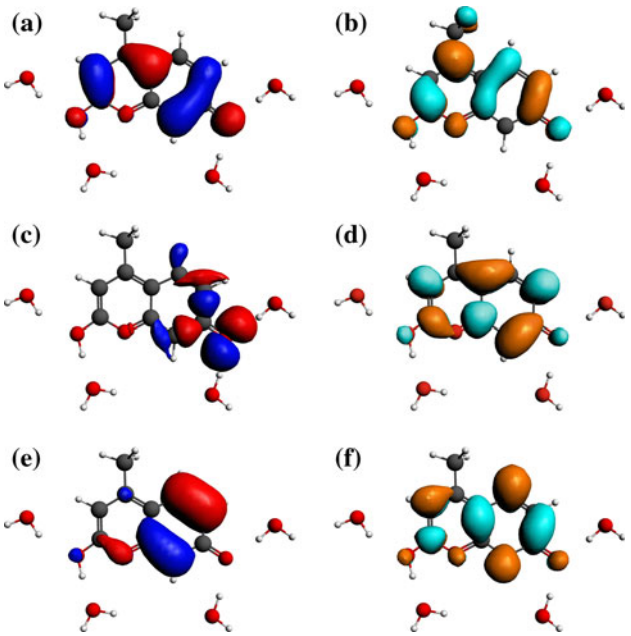

Fig. 8 The embedded orbitals in keto-7-hydroxy-4-methylcoumarin-$(H_2O)_4$ complex, which provide the dominant contributions to the lowest excitations: **a** HOMO, **b** LUMO, **c** HOMO−1, **d** LUMO+1, **e** HOMO−2, and **f** LUMO+2

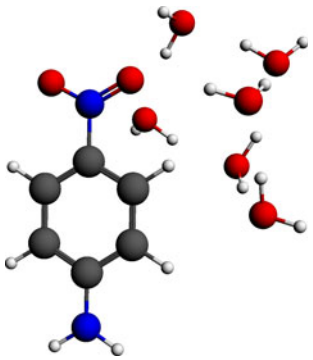

Fig. 9 *P*-Nitro aniline-$(H_2O)_6$ complex

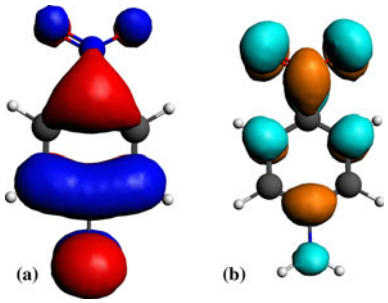

Fig. 10 The pair of molecular orbitals in isolated *P*-nitro aniline, which provides the dominant contribution to the lowest excitation: **a** HOMO, **b** LUMO

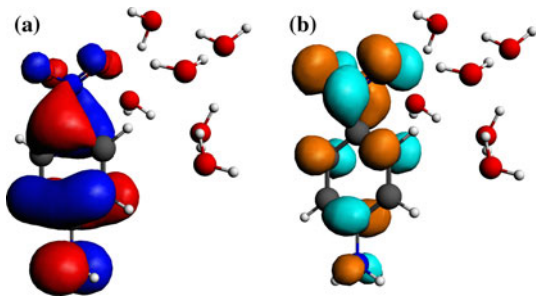

Fig. 11 The pair of molecular orbitals in the *P*-nitro aniline–$6H_2O$ complex, which provides the dominant contribution to the lowest excitation: **a** HOMO, **b** LUMO

theoretically [95–97] due to its remarkable photophysical properties. The theoretical investigations of this molecules have helped to solve the ambiguity of nature of excitation [98]. The keto form of 7H4MC in a cluster comprising four water molecules is shown in Fig. 6. The ground-state geometry of the complex is chosen from Ref. [98] to study the sensitivity of the FDET excitation energy shifts for the choice for ρ_B. Three lowest transitions (two $\pi \rightarrow \pi^*$ and one $n \rightarrow \pi^*$ excitations) are reported in Table 5. For subsystem A, STO–aug-TZP basis set and the SAOP [84, 85] approximation for the exchange-correlation potential is

used for all calculations in this subsection. ρ_B on the other hand is generated using several STO type atomic basis sets and three different approximations for the exchange-correlation potential.

The orbitals for isolated and embedded chromophore are shown in Figs. 7 and 8, respectively. The analyzed excitations are dominated by the following transitions: $\pi \rightarrow \pi^*(1)$ (HOMO to LUMO), $\pi \rightarrow \pi^*(2)$ (HOMO to LUMO−1), and $n \rightarrow \pi^*$ (HOMO−1 to LUMO). In line with the trends observed for embedded *cis*-7-hydroxyquinoline reported in the previous section, the shifts of the excitation energies depend weakly on the dipole moment of the environment provided the STO–DZ or larger basis set is used in generation of ρ_B (see Table 5).

3.2.2 Microsolvated P-nitro aniline

For *P*-nitro aniline (PNA) in six water molecules three local excitations are analyzed: the lowest singlet (S), and triplet (T) $\pi \rightarrow \pi^*$. The geometry of the complex was taken

Table 6 Excitation energies (ε) and environment-induced spectral shifts ($\Delta\varepsilon$) of a lowest singlet and triplet excitations obtained using different choices for ρ_B (Kohn–Sham calculations with three choices for exchange-correlation potentials and four choices for the basis sets) for the PNA with six H_2O molecules. The corresponding excitation energy for isolated chromophore are: $\varepsilon_{\pi\rightarrow\pi^*(S)} = 3.3622$ eV, $\varepsilon_{\pi\rightarrow\pi^*(T)} = 2.5086$ eV, and the corresponding dipole moment (in Debye units) of the environment is also given

Generation of ρ_B		Excitation energy (eV)		Spectral shift (cm^{-1})		μ_B (Debye)
Xc-potential	Basis set	$\varepsilon_{\pi\rightarrow\pi^*(S)}$	$\varepsilon_{\pi\rightarrow\pi^*(T)}$	$\Delta\varepsilon_{\pi\rightarrow\pi^*(S)}$	$\Delta\varepsilon_{\pi\rightarrow\pi^*(T)}$	
SAOP	STO–SZ	3.2549	2.3546	−865	−1242	2.52
	STO–DZ	3.2245	2.3292	−1111	−1447	3.39
	STO–DZP	3.2678	2.3611	−761	−1190	2.54
	STO–TZP	3.2653	2.3624	−782	−1179	2.56
	STO–TZ2P	3.2631	2.3615	−799	−1186	2.57
	STO–aug-TZP	3.2576	2.3603	−844	−1196	2.58
PBE	STO–SZ	3.2639	2.3647	−793	−1161	2.29
	STO–DZ	3.2265	2.3198	−1095	−1523	3.18
	STO–DZP	3.2523	2.3703	−886	−1115	2.35
	STO–TZP	3.2647	2.3700	−786	−1118	2.39
	STO–TZ2P	3.2676	2.3688	−763	−1127	2.40
	STO–aug-TZP	3.2668	2.3727	−769	−1096	2.41
LDA	STO–SZ	3.2523	2.3604	−886	−1195	2.41
	STO–DZ	3.2227	2.3280	−1125	−1457	3.35
	STO–DZP	3.2672	2.3736	−766	−1089	2.44
	STO–TZP	3.2626	2.3731	−803	−1093	2.48
	STO–TZ2P	3.2481	2.3723	−920	−1099	2.49
	STO–aug-TZP	3.2688	2.3760	−753	−1069	2.48

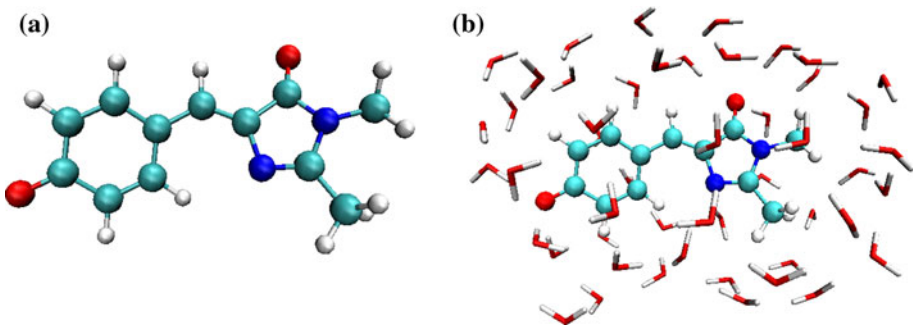

Fig. 12 Isolated (*left*) and hydrated by 49 water molecules (*right*) 4-hydroxybenzylidene-2,3-dimethylimidazolinone anion

Table 7 Dependence of the two lowest electronic excitation energies (ε_1 and ε_2) and the corresponding spectral shifts ($\Delta\varepsilon_1$ and $\Delta\varepsilon_2$) on the basis set choices for generating the Kohn–Sham electronic density of the solvent. The corresponding electronic excitation energies of isolated chromophore are: ε_1 = 2.3827 eV and ε_2 = 2.9291 eV. The corresponding dominant molecular orbital (MO) transitions are HOMO-1 → LUMO for ε_1 and HOMO → LUMO for ε_2. The magnitude of the dipole moment of the environment is also given

Basis set for ρ_B	Excitation energy (eV)		Spectral shift (cm^{-1})		μ_B (Debye)
	ε_1	ε_2	$\Delta\varepsilon_1$	$\Delta\varepsilon_2$	
STO–SZ	2.7907	3.0142	3291	686	11.72
STO–DZ	3.0054	3.0508	5022	982	13.24
STO–DZP	2.9742	3.0340	4771	846	10.66
STO–TZP	2.9605	3.0318	4660	828	10.78
STO–TZ2P	2.9556	3.0306	4621	819	10.81
STO–aug-TZP	2.9415	3.0289	4507	805	10.79

from Ref. [99] and is shown in Fig. 9. The π and π^* orbitals are shown in Figs. 10 and 11 for isolated chromophore and complex respectively. These are HOMO and LUMO for both isolated and embedded PNA. Table 6 collects the excitation energies and solvatochromic shifts for singlet and triplet $\pi \rightarrow \pi^*$ transition. The excitation energies and solvatochromic shifts for both the transitions do not vary significantly with the change of basis set or exchange correlation functional. The FDET shifts evaluated using ρ_B obtained with the STO–DZP or any larger basis set are numerically equivalent.

3.2.3 *Hydrated 4-hydroxybenzylidene-2,3-dimethylimidazolinone anion*

In this subsection, the estimation of the sensitivity of the calculated shifts on ρ_B is made for a realistic model of a chromophore in water solvent, following the same procedure as the one used in the previous subsection. The chromophore investigated is 4-hydroxybenzylidene-2,3-dimethylimidazolinone (HBDI) anion, which is the chromophore in green fluorescent protein. The cluster used for the calculations consists of the HBDI anion in the *cis* conformation and 49 water molecules (see Fig. 12), which geometry is taken from Ref. [100]. The water molecules in the cluster represents the complete first solvation shell.

STO–DZP basis sets are used for the HBDI anion. The non-additive kinetic potential in Eq. 3 is approximated using the NDSD bi-functional [64]. ρ_B is obtained from Kohn–Sham calculations for isolated subsystem *B* applying the LDA exchange-correlation functional and various types of STO orbitals (SZ, DZ, DZP, TZP, TZ2P, and aug-TZP).

Table 7 shows the dependence of the two lowest electronic excitation energies (ε_1 and ε_2) and the corresponding spectral shifts ($\Delta\varepsilon_1$ and $\Delta\varepsilon_2$) on the basis set choices for generating the Kohn–Sham electronic density of the solvent. The corresponding dominant molecular orbital (MO) transitions are HOMO-1 → LUMO for ε_1 and HOMO → LUMO for ε_2. The involved orbitals (both isolated and solvated HBDI anion) are shown in Fig. 13.

The results collected in Table 7 indicate that, starting from STO–DZP, increasing further the basis sets does not affect significantly the calculated spectral shifts.

The solvated 4-hydroxybenzylidene-2,3-dimethylimidazolinone anion is the largest system investigated in the present work. The CPU timings of the FDET calculations for this system are collected in Table 8 to illustrate the main computational advantage of the FDET-based methods. Solving LR-TDDFT equations for getting excitation energies requires the same time regardless which method is used to generate ρ_B (The exceptions for the last two lines in Table 8 originate from different number of iterations in the Davidson procedure to diagonalize the largest matrix in LR-TDDFT calculations. In this particular case, ρ_B is

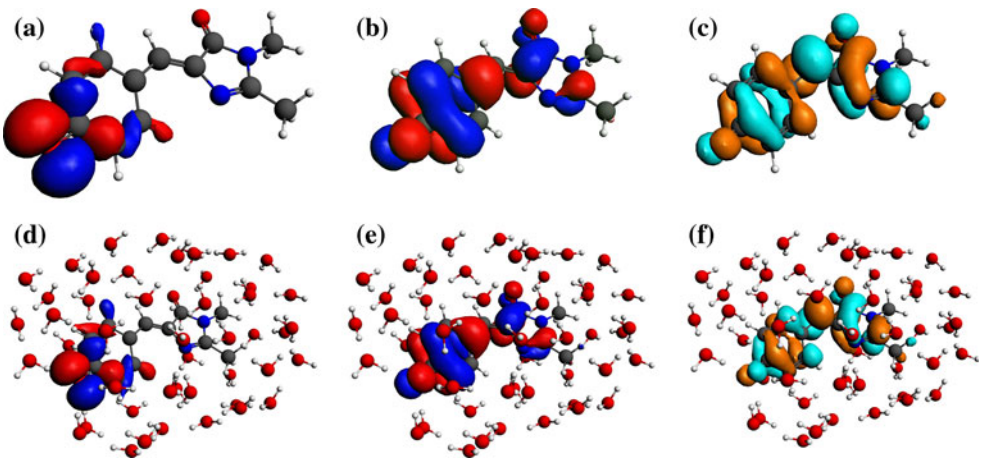

Fig. 13 The molecular orbitals, which provide the dominant contributions to the lowest two excitations. **a** HOMO−1, **b** HOMO, and **c** LUMO for the isolated 4-hydroxybenzylidene-2,3-dimethylimidazolinone (HBDI) anion; **d** HOMO−1, **e** HOMO, and **f** LUMO for the embedded HBDI anion

Table 8 The dependence of the CPU time[a] (hour:minute) of FDET calculations on the choice of basis sets used to generate ρ_B for 4-hydroxybenzylidene-2,3-dimethylimidazolinone anion in the environment consisting 49 water molecules

Basis set for ρ_B	Generation of ρ_B	FDET (ground state)	FDET/LR-TDDFT (excited state)	Total
STO–SZ	00:03	00:18	00:17	00:39
STO–DZ	00:05	00:33	00:16	00:55
STO–DZP	00:13	01:22	00:17	01:54
STO–TZP	00:17	01:36	00:16	02:10
STO–TZ2P	00:33	02:06	00:51[b]	03:30
STO–aug-TZP	01:28	03:03	00:25	04:56

[a] Each calculation is run on one node consisting of eight 3.0 GHz cores

[b] The CPU time is proportional to the number of iterations in the Davidson procedure to diagonalize the largest matrix in LR-TDDFT calculations

obtained by using ground-state Kohn–Sham calculations whereas the excited-state calculations involve the same space of occupied and unoccupied orbitals). In contrast with solving Casida's equations for excited-state FDET calculations, the time needed for ground-state FDET calculations increases with the basis set size for ρ_B. This is rather a specific feature of the ADF program concerning the evaluation of the Coulomb terms, the timing of which depends on the site of the orbital- and auxiliary- basis sets used for ρ_B. Concerning the generation of ρ_B, its scaling reflects the conventional implementation of the Kohn–Sham calculations.

4 Conclusions

According to FDET, every observable calculated at a given choice for ρ_B is a functional of ρ_B. The unique correspondence between the observable of interest and ρ_B involves the embedding potential defined in Eq. 3 which changes if ρ_B changes. The present work concerns these correspondences for a particular case of energies of local excitations which are evaluated by means of applying FDET within LR-TDDFT framework. In such calculations, the shifts are determined by the embedding potential (and its functional derivative with respect to ρ_A). The examples provided in the present work form a series constructed to address the issue: *How simple can be the method to generate ρ_B in hydrogen bonded clusters without significant deterioration of the calculated shifts in energies of local excitations?* The following conclusions/recommendations emerge from the reported studies on various organic chromophores, excitations, and hydrogen-bonded environments. Generating ρ_B as a superposition of spherically symmetric atomic charges, which was shown to be adequate in environments being ionic crystals, does not seem to be robust enough for environments consisting of molecules. The FDET excitation energies results depend critically on the choice of net atomic charges. The example of ammonia-7HQ complex shows that none of the commonly used techniques to assign atomic net charges in a molecule is applicable. This originates probably from the fact that such simple approximation is incapable of reproducing the directional character of atoms with lone pairs. Generating ρ_B as a superposition of molecular densities is a more reliable strategy but still might lead to relative errors in the shifts exceeding 25 %. Such errors occur if the molecules within the environment interact strongly with each other as in the shown examples of environments consisting of hydrogen-bonded chains of molecules. The most robust strategy to generate ρ_B emerging from the present study consists of using less expensive Kohn–Sham calculations for the whole environment (or at least for all molecules near the chromophore). STO–DZP basis set or larger and any among the three investigated exchange-correlation potentials (LDA, PBE, or SAOP) lead to similar results. The relative shift vary usually less than 0.02 eV (or about 150 cm^{-1}) whereas the relative excitation energy shifts change by no more than 10 % regardless which approximation for the exchange-correlation potential is used or which basis set (STO–DZP or larger) is used. These results can be considered as estimations of errors made due to arbitrary choices of ρ_B made in multi-scale computer simulations based on FDET.

The embedding potential given in Eq. 3 applies not only for embedding a non-interacting reference system, which is considered in the present work, but also for methods using other quantum mechanical descriptors for ρ_A as shown in Ref. [22, 23]. Such FDET-based simulations are gaining increasing popularity [24–29, 31–33]. The effect of varying ρ_B on the embedding potential and subsequently for shifts in excitation energies (and other observables directly related to the electronic structure of subsystem *A*) can be expected to be similar for such methods.

Concerning the relative stability of FDET calculated shifts in energies of local excitations with respect to the choices for ρ_B, we underline that in the commonly used methods of the QM/MM type, the embedding potential comprises ONLY electrostatic component. Therefore, the embedded wavefunction or other quantum mechanical descriptor obtained in such calculations depends critically on the distribution of charges and higher electric moments in the environment. Including or not the electrostatic field generated by the induced dipole moments on atoms in the environment might affect the results significantly. The present work shows that, in the FDET calculations which

are based on variational principle, the results depend less on the choice for ρ_B. Several cases, where two choices for the density of the environment differing in the dipole moment by more than 10 % lead to almost identical shifts in the excitation energy, are reported in the present work. We interpret this robustness of the FDET calculated excitation energy shifts with respect to the choice of the density of the environment (ρ_B) as originating in the variational character of FDET and the existence of multiple pairs of ρ_A and ρ_B adding up to the same total density in the case of exact theory. This numerical result shows that the use of the notion of "polarization of the environment by the embedded subsystem" might be misleading in the FDET calculations at least for such weak interactions as the hydrogen bond between the chromophore and the molecule in the environment.

Finally, it is worthwhile noticing that performing FDET-based simulations for excited states of embedded chromophores as an alternative to treat the whole system at the same quantum mechanical level leads to significant computational savings which result from two approximations: (a) neglect of dynamic response of the environment and (b) the use of inexpensive methods to generate the ρ_B—a ground-state Kohn–Sham electron density for instance. None of them is general. The first approximation leads to the reduction of the number of Kohn–Sham orbitals (occupied and unoccupied) in solving LR-TDDFT equations and is applicable in the absence of overlap in the energy levels in the two subsystems. In such cases going beyond NDRE is indispensable [46]. The second approximation is also not general. The present work, indicates that using inexpensive Kohn–Sham-based methods to generate ρ_B such as using local-density approximation for exchange-correlation potential and STO–DZP basis set, seems a universally adequate approximation for hydrogen-bonded environments. This general recommendation complements our conclusions emerging from studies concerning other environments such as ionic solids [38] or cases where confinement dominate the environment-induced shifts of properties of embedded molecules [34], for which it was found that approximating the density of the solid by a sum of ionic densities is an adequate approximation.

5 Supporting information

Results obtained with other basis sets, numerical values of excitation energies.

Acknowledgments Grants from Swiss National Science Foundation (200020/134791/1 FNRS) and COST (CODECS) are greatly appreciated.

References

1. Åquist J, Warshel A (1993) Chem Rev 93:2523
2. Bakowies D, Thiel W (1996) J Phys Chem 100(25): 10580–10594
3. Sauer J, Ugliengo P, Garrone E, Sounders VR (1994) Chem Rev 94:2095
4. Cramer CJ, Truhlar DG (1999) Chem Rev 99(8):2161–2200
5. Gordon MS, Fedorov DG, Pruitt SR, Slipchenko LV (2012) Chem Rev 112(1):632–672
6. Zheng H (1993) Phys Rev B 48:14868–14883
7. Laio A, VandeVondele J, Rothlisberger U (2002) J Chem Phys 116(16):6941–6947
8. Fradelos G, Wesolowski TA (2011) J Phys Chem A 115(35):10018–10026
9. Fradelos G, Wesolowski TA (2011) J Chem Theory Comput 7(1):213–222
10. Sanchez ML, Aguilar MA, Olivares del Valle FJ (1997) J Comput Chem 18(3):313–322
11. Coutinho K, Georg HC, Fonseca TL, Ludwig V, Canuto S (2007) Chem Phys Lett 437(1–3):148–152
12. Casanova D, Gusarov S, Kovalenko A, Ziegler T (2007) J Chem Theory Comput 3(2):458–476
13. Engkvist O, strand P-O, Karlstrm G (2000) Chem Rev 100(11):4087–4108
14. Nanda KD, Beran GJO (2012) J Chem Phys 137(17)
15. Gresh N, Cisneros GA, Darden TA, Piquemal J-P (2007) J Chem Theory Comput 3(6):1960–1986
16. Day PN, Jensen JH, Gordon MS, Webb SP, Stevens WJ, Krauss M, Garmer D, Basch H, Cohen D (1996) J Chem Phys 105(5): 1968–1986
17. Assfeld X, Rivail JL (1996) Chem Phys Lett 263(1–2):100–106
18. Winter NW, Pitzer RM, Temple DK (1987) J Chem Phys 86(6):3549–3556
19. Moriarty JA, Phillips R (1991) Phys Rev Lett 66(23):3036–3039
20. Wesolowski TA, Warshel A (1993) J Phys Chem 97(30): 8050–8053
21. Wesolowski TA (2006) One-electron equations for embedded electron density: challenge for theory and practical payoffs in multi-level modelling of soft condensed matter. In: Leszczynski J (ed) Computational chemistry: reviews of current trends, vol X. World Scientific, Singapore, pp 1–82
22. Wesolowski TA (2008) Phys Rev A 77(1):012504(1–8)
23. Pernal K, Wesolowski TA (2009) Int J Quant Chem 109(11, Sp. Iss. SI):2520–2525
24. Stefanovich EV, Truong TN (1996) J Chem Phys 104(8): 2946–2955
25. Govind N, Wang YA, da Silva AJR, Carter EA (1998) Chem Phys Lett 295(12):129–134
26. Trail JR, Bird DM (2000) Phys Rev B 62(24):16402–16411
27. Hodak M, Lu W, Bernholc J (2008) J Chem Phys 128:014101
28. Neugebauer J, Baerends EJ (2006) J Phys Chem A 8786–8796
29. Lahav D, Kluner T (2007) J Phys Cond Matt 19:226001
30. Neugebauer J (2010) Phys Rep 489:1-87
31. Gomes ASP, Jacob CR, Visscher L (2008) Phys Chem Chem Phys 10:5353
32. Roncero O, de Lara-Castells MP, Villarreal P, Flores F, Ortega J, Paniagua M, Aguado A (2008) J Chem Phys 129(18):184104
33. Goodpaster Jason D, Ananth Nandini, Manby Frederick R, Miller Thomas F III (2010) J Chem Phys 133(8):084103
34. Wesolowski TA (1999) Chem Phys Lett 311(1–2):87–92
35. Hong GY, Strajbl M, Wesolowski TA, Warshel A (2000) J Comput Chem 21(16):1554–1561
36. Zbiri M, Atanasov M, Daul C, Garcia-Lastra JM, Wesolowski TA (2004) Chem Phys Lett 397(4–6):441–446

37. Wesolowski TA (2004) J Am Chem Soc 126(37):11444–11445
38. Zhou X, Wesolowski Tomasz A, Tabacchi G, Fois E, Calzaferri G, Devaux A (2013) Phys Chem Chem Phys 15:159–167
39. Neugebauer J, Louwerse MJ, Baerends EJ, Wesolowski TA (2005) J Chem Phys 122(9):094115
40. Jacob CR, Visscher L (2006) J Chem Phys 125:194104
41. Jacob CR, Beyhan SM, Visscher L (2007) J Chem Phys 126:234116
42. Gotz AW, Beyhan SM, Visscher L (2009) J Chem Theory Comput 5(12):3161–3174
43. Kiewisch K, Eickerling G, Reiher M, Neugebauer J (2008) J Chem Phys 128(4):044114(1–15)
44. Casida ME (1995) Time-dependent density-functional response theory for molecules. In: Chong DP (ed) Recent advances in density-functional methods. World Scientific, Singapore
45. Casida ME, Wesolowski TA (2004) Int J Quantum Chem 96(6):577–588
46. Neugebauer J (2007) J Chem Phys 97:134116
47. Fradelos G, Lutz JJ, Wesolowski TA, Piecuch P, Woch M (2011) J Chem Theory Comput 7(6):1647–1666
48. Hohenberg P, Kohn W (1964) Phys Rev 136(3B):B864–B871
49. Elliott P, Cohen MH, Wasserman A, Burke K (2009) J Chem Theory Comput 5(4):827–833
50. Elliott P, Burke K, Cohen MH, Wasserman A (2010) Phys Rev A 82:024501
51. Kohn W, Sham LJ (1965) Phys Rev 140(4A):A1133–A1138
52. Severo Pereira Gomes A, Jacob CR (2012) Annu Rep Prog Chem Sect C Phys Chem 108:222–277
53. Levy M (1979) Proc Natl Acad Sci U S A 76(12):6062–6065
54. Levy M (1982) Phys Rev A 26(3):1200–1208
55. Tran F, Wesolowski TA (2003) J Chem Phys 118:2072–2080
56. Thomas LH (1927) Proc Camb Philos Soc 23:542
57. Fermi E (1928) Z Phys 48:73
58. von Weizsäcker CF (1935) Z Phys 96:431
59. Kirzhnits DA (1957) Sov Phys JETP 5:64
60. Wesolowski TA, Weber J (1997) Int J Quantum Chem 61(2):303–311
61. Wesolowski TA, Chermette H, Weber J (1996) J Chem Phys 105(20):9182–9190
62. Wesolowski TA (1997) J Chem Phys 106(20):8516–8526
63. Lembarki A, Rogemond F, Chermette H (1995) Phys Rev A 52(5):3704–3710
64. Garcia Lastra JM, Kaminski JW, Wesolowski TA (2008) J Chem Phys 129(7):074107(1–15)
65. Wesolowski TA, Weber J (1996) Chem Phys Lett 248(1–2): 71–76
66. Bernard YA, Dulak M, Kaminski JW, Wesolowski TA (2008) J Phys A Math Theor 41(5):055302(1–19)
67. Fux S, Kiewisch K, Jacob CR, Neugebauer J, Reiher M (2008) . Chem Phys Lett 461(46):353–359
68. Fux S, Jacob CR, Neugebauer J, Visscher L, Reiher M (2010) J Chem Phys 132(16):164101(1–18)
69. Huang C, Pavone M, Carter EA (2011) J Chem Phys 134(15):154110(1–11)
70. Cortona P (1991) Phys Rev B 44(16):8454–8458
71. Wesolowski TA (2005) Mol Phys 103(6-8):1165–1167
72. Savin A, Wesolowski TA (2009) Prog Theor Chem Phys 19:327–339
73. Savin A, Wesolowski TA (2013) Non-additive kinetic energy and potential in analytically solvable systems and their approximate counterparts. In: Wesolowski TA, Wang YA (eds) Recent progress in orbital-free density functional theory. Recent Progress in Computational Chemistry, vol 6. World Scientific, Singapore, pp 275–295
74. de Silva P, Wesolowski TA (2012) J Chem Phys 137(9):094110
75. Gritsenko OV (2013) On the principal difference between the exact and approximate frozen-density embedding theory. In: Wesolowski TA, Wang YA (eds) Recent progress in computational chemistry, vol 6. World Scientific, Singapore, pp 355–365
76. Dulak M, Wesolowski TA (2006) J Chem Phys 124:164101
77. Fradelos G, Lutz JJ, Wesolowski TA, Piecuch P, Wloch M (2012) Shifts in excitation energies induced by hydrogen bonding: A comparison of the embedding and supermolecular time-dependent density functional theory calculations with the equation-of-motion coupled-cluster results. In: Hoggan PEE, Brandas EJJ, Maruani J, Piecuch P, Delgado-Barrio G (eds) Advances in the theory of quantum systems in chemistry and physics. Progress in theoretical chemistry and physics, vol 22. Springer, Netherlands, pp 219–248
78. Wesolowski T, Warshel A (1994) J Phys Chem 98(20): 5183–5187
79. Wesolowski T, Muller RP, Warshel A (1996) J Phys Chem 100(38):15444–15449
80. Adf, scm, theoretical chemistry. Vrije Universiteit, Amsterdam, the Netherlands. http://www.scm.com
81. Dulak M, Wesolowski TA (2005) Int J Quantum Chem 101(5):543–549
82. Jacob CR, Neugebauer J, Visscher L (2008) J Comput Chem 29:1011
83. van Lenthe E, Baerends EJ (2003) J Comput Chem 24(9): 1142–1156
84. Gritsenko OV, Schipper PRT, Baerends EJ (1999) Chem Phys Lett 302(34):199–207
85. Schipper PRT, Gritsenko OV, van Gisbergen SJA, Baerends EJ (2000) J Chem Phys 112(3):1344–1352
86. Perdew JP (1991) Electronic structure of solids'91, vol X. Academie Verlag, Berlin
87. Fradelos G, Kaminski JW, Wesolowski TA, Leutwyler S (2009) J Phys Chem A 113:9766
88. Mulliken RS (1955) J Chem Phys 23:1833–1840
89. Hirschfeld FL (1977) Theor Chim Acta 44:129–138
90. Baerends EJ, Bickelhaupt FM, Guerra CF, Handgraaf JW (2003) J Comp Chem 25:189–210
91. Snijders JG, Swart M, Van Duijnen PTh (2001) J Comp Chem 22:79–88
92. Dirac PAM (1930) Proc Camb Philos Soc 26:376–385
93. Vosko SH, Wilk L, Nusair M (1980) Can J Phys 58(8): 1200–1211
94. Perdew JP, Burke K, Ernzerhof M (1997) Phys Rev Lett 78(7):1396–1396
95. Seixas de Melo J, Fernandes PF (2001) J Mol Struct 565–566: 69–78
96. Novak I, Kovač B (2001) J Phoochem Photobiol 113:913
97. Kovač B, Novak I (2002) Spectrochim Acta A 58:14831488
98. Georgieva I, Trendafilova N, Aquino A, Lischka H (2005) J Phys Chem A 109:11860–11869
99. Slipchenko LV (2010) J Phys Chem A 114:8824–8830
100. Polyakov I, Epifanovsky E, Grigorenko B, Krylov AI, Nemukhin A (2009) J Chem Theory Comput 5(7):1907–1914